NASA CR 54820
AGC 8800-52

AERODYNAMIC DESIGN
MODEL II TURBINE
M-1 FUEL TURBOPUMP ASSEMBLY

By

T. W. Reynolds

Prepared for

National Aeronautics and Space Administration

Contract NAS 3-2555

AEROJET-GENERAL CORPORATION

SACRAMENTO, CALIFORNIA

Requests for copies of this report should be referred to:

National Aeronautics and Space Administration
Office of Scientific and Technical Information
Attention: AFSS-A
Washington, D. C. 20546

NASA CR-54820
AGC 8800-52

TECHNOLOGY REPORT

AERODYNAMIC DESIGN
MODEL II TURBINE
M-1 FUEL TURBOPUMP ASSEMBLY

Prepared for

NATIONAL AERONAUTICS AND SPACE ADMINISTRATION

April 15, 1966

CONTRACT NAS 3-2555

Prepared by
AEROJET-GENERAL CORPORATION
LIQUID ROCKETS OPERATION
SACRAMENTO, CALIFORNIA

AUTHOR: T. W. Reynolds

APPROVED: W. E. Campbell,
Manager
M-1 Turbopump Project

Technical Management
NASA LEWIS RESEARCH CENTER
CLEVELAND, OHIO

TECHNICAL MANAGER: W. W. Wilcox

APPROVED: W. F. Dankhoff
M-1 Project Manager

ABSTRACT

22268

A two-row Curtis staged turbine was designed as a direct drive for the M-1 liquid hydrogen turbopump. The design-point calculated shaft output is 88,150 horsepower at 13,225 rpm. The estimated turbine efficiency is 62.8% at a velocity ratio of 0.188. The mean blade diameter is 23.0-in., giving a tip speed of 1490 ft/sec.

TABLE OF CONTENTS

LIST OF TABLES

LIST OF FIGURES

I. SUMMARY

This report describes the aero-thermodynamic design of the Curtis turbine used to drive the liquid hydrogen turbopump for the M-1 engine. At the design point, the turbine is capable of developing 88,150 horsepower at an estimated over-all efficiency of 62.8% based upon the ratio of the total inlet pressure at the nozzles to the static discharge pressure. The losses from the turbine manifold inlet flange to the nozzle inlet are estimated to be 1.6 points of the over-all efficiency, which reduces the efficiency to 61.2%.

The design point specifications for the turbine are listed in Table I.

TABLE I

M-1 LIQUID HYDROGEN PUMP TURBINE DESIGN PARAMETERS

Inlet Total Pressure at Manifold Inlet Flange	psia	1020
Inlet Total Pressure at Nozzle Inlet	psia	1000
Inlet Total Temperature at Nozzle Inlet	°R	1460
Discharge Static Pressure	psia	214
Pressure Ratio, Total to Static	--	4.673
Gas Weight Flow Rate	lbm/sec	99.33
Speed	rpm	13,225
Mean Diameter of Blading (at 68°F, 0 rpm)	in.	23.0
Blade Speed at Mean Diameter	ft/sec	1327
Blade-Jet Speed Ratio	--	0.188

II. INTRODUCTION

The pumping system for the liquid propellants used in the M-1 engine consists of two separate turbopumps, each driven by a Curtis turbine. The turbines are supplied with hot gas by a gas generator. This hot gas is the combustion products of the liquid hydrogen and the liquid oxygen. The turbines are arranged in a series with the gas initially expanded in the fuel turbine and then further expanded in the oxidizer turbine. The exhaust gas from the oxidizer turbine is routed through three heat exchangers; one exchanger is utilized to heat the hydrogen for the gimbal actuators, another heats the hydrogen for tank pressurization, and the third heats the oxygen for tank pressurization. The exhaust gas is then directed to the lower skirt of the thrust chamber to cool the walls. Finally, the gas is ejected through a set of small nozzles which provides an approximate specific impulse of 260 lbf-sec/lbm (see Figure No. 1).

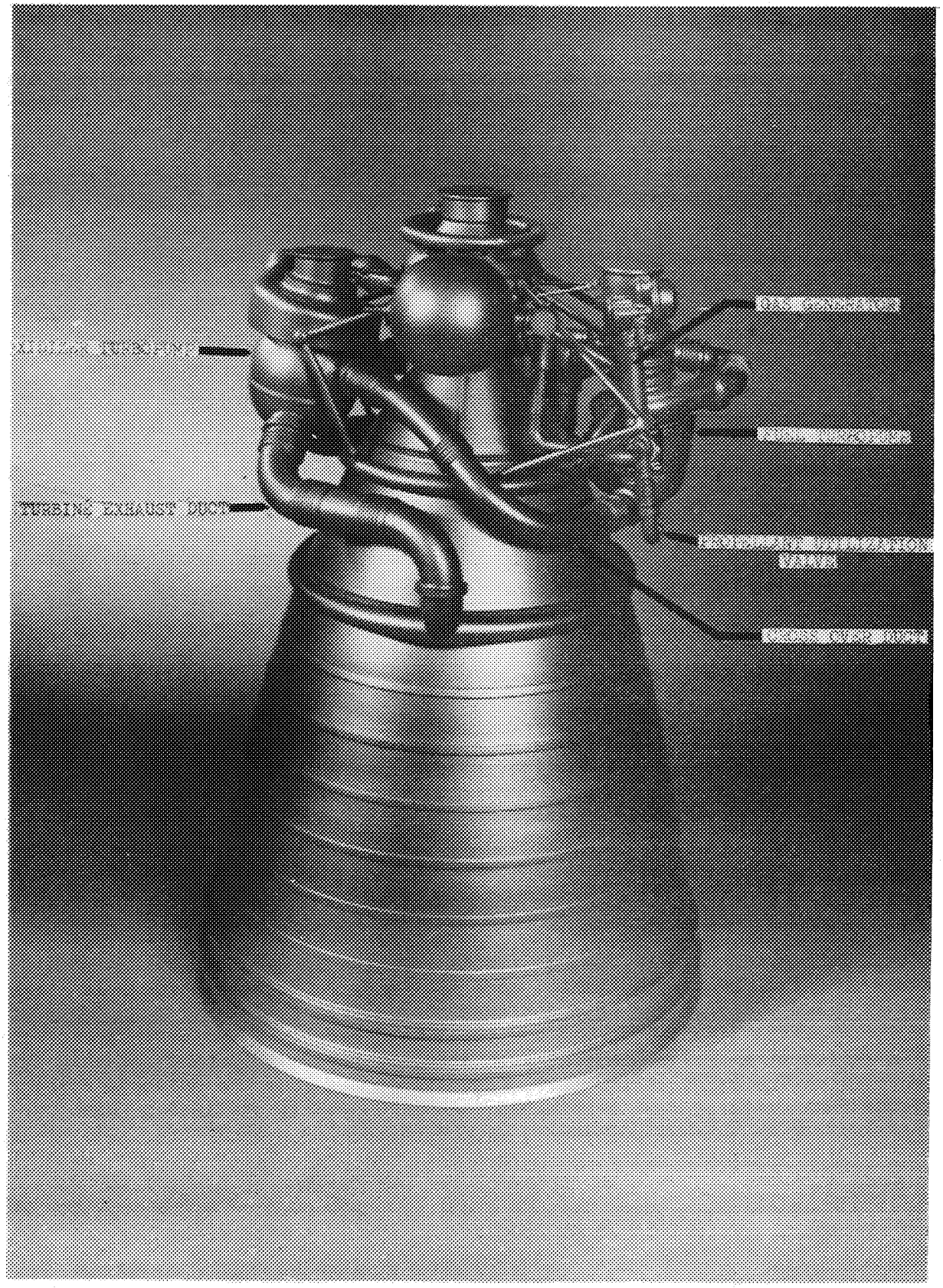

Figure 1. M-1 Engine Mockup

The operating cycle of the engine is initiated by discharging helium gas directly into the fuel turbine inlet manifold. This causes rotation of the fuel turbopump rotor, and in turn, the oxidizer turbopump rotor, at a speed that is sufficient to furnish propellants to the gas generator. The gas generator is ignited at a predetermined pressure, to complete the bootstrapping operation. Now, both turbines quickly reach operating speeds thus furnishing the fuel and oxidizer to the thrust chamber injector.

Some of the more significant mechanical design features are shown in Figure No. 2. The turbine components are fabricated almost entirely of Inconel 718 which is an age hardenable nickel-chromium alloy. This material is very ductile and can easily be welded by the Tungsten Inert Gas (TIG) or electron beam methods. It also retains a high strength at both cryogenic and elevated temperatures (-420 to +1300°F). With Inconel 718, thin walled housings and narrow flanges can be used which reduce the thermal-induced stresses. The mechanical design is detailed in a separate report.(1)

The two-stage Curtis turbine was specified for use in the M-1 fuel turbopump. A full scale turbine of this configuration has not been tested under hot-firing conditions. However, at the NASA Lewis Research Center, by using cold air, actual experimental performance data for the inlet manifold, turbine nozzles, and the complete two-stage turbine have been obtained with a subscale model. The results of these tests will be reported separately by the National Aeronautics and Space Administration.

The design and development of this turbine was conducted by the Aerojet-General Corporation under a contract with the National Aeronautics and Space Administration.

Dr. M. H. Vavra, a consultant from the U. S. Naval Post-Graduate School at Monterey, California,(2) was responsible for the aerodynamic design of the unit. The results of his analysis are used extensively in this report. The analysis for the velocity distribution of the blade and vane profiles was accomplished by the Aerojet-General Corporation, using the National Aeronautics and Space Administration computer program.(3)

---

(1) Reynolds, T. W., The Mechanical Design of a Two-Stage Impulse Turbine for the Liquid Hydrogen Turbopump of the M-1 Engine, NASA Report CR-54821, 22 April 1966 (Aerojet-General Corporation Report No. 8800-58).

(2) Vavra, M. H., M-1 Fuel Turbine, Aerodynamic Design, RMR No. 0143, Aerojet-General Corporation, November 1963.

(3) Stinson, W. D., Turbine Computer Program, NASA-Aerojet Computer Job No. 1009, Aerojet-General Corporation Memorandum, dated 27 September 1962.

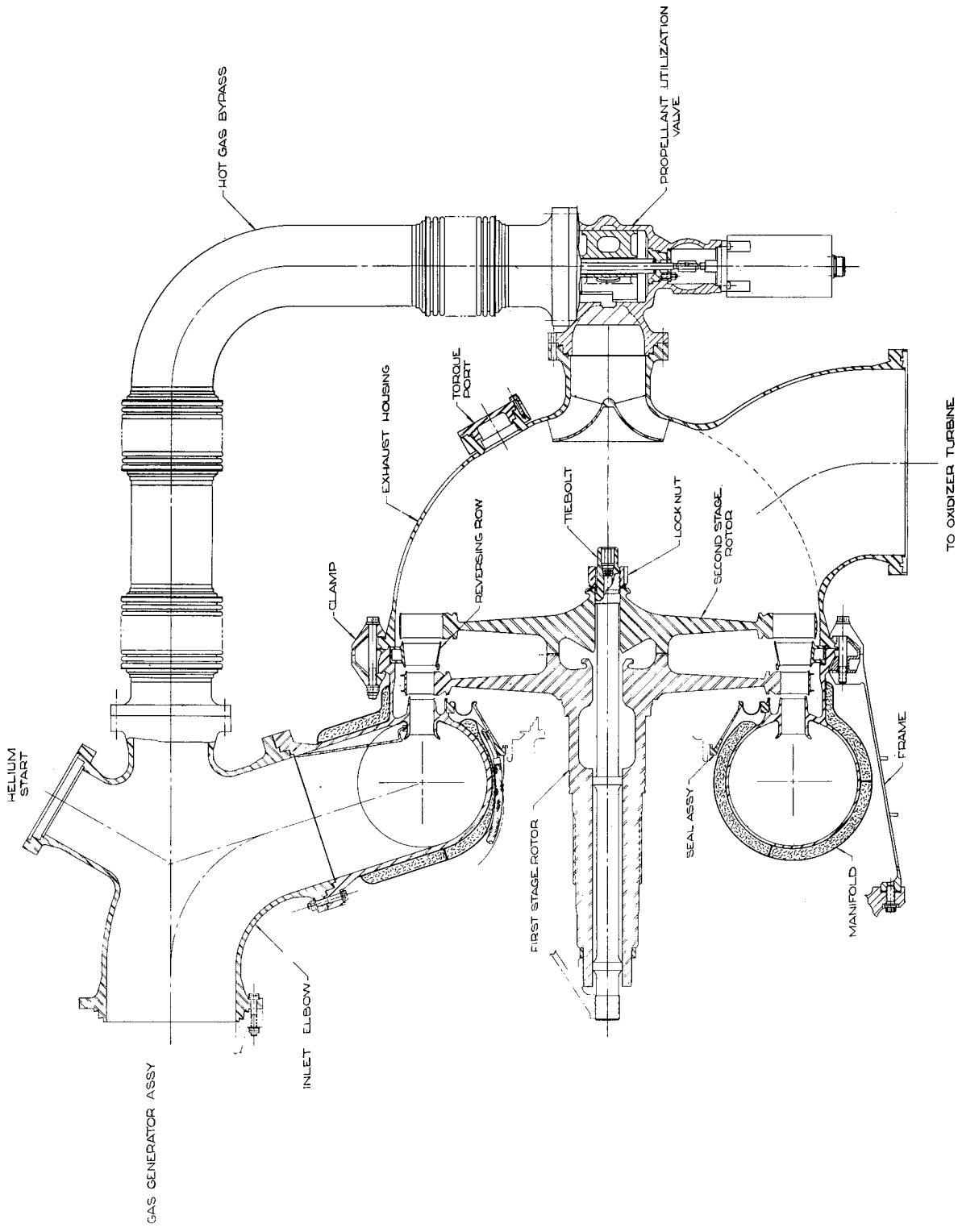

Figure 2. Fuel Turbine Components in Cross-Section

III. TURBINE DESIGN

A. DESIGN PHILOSOPHY

The fuel turbine for the M-1 engine must accomplish an isentropic enthalpy drop of 999 BTU/lbm. The peripheral speed at the mean diameter was limited to approximately 1350 ft/sec. Impulse turbines are capable of obtaining operating efficiencies of about 76% without recovery of the leaving velocity head and about 81% with recovery of the leaving velocity head. To obtain operating efficiencies of 76 to 81% with any isentropic enthalpy drop of 999 BTU/lbm would require five to six stages. By comparison, a single stage impulse turbine would not exceed an efficiency of approximately 49%.

Because an outboard bearing was not acceptable in the M-1 turbopump design, a five-stage turbine was not practical. This results from the large overhang with the inboard bearings and the critical speed problems which are a consequence.

The compromise selected between a multistage impulse turbine which operates at a high degree of efficiency and a single stage unit with a low degree of efficiency is the two-row Curtis turbine. Originally, Curtis stages were designed as pure velocity stages where the gas is expanded to the discharge pressure in the first nozzle. However, experience has shown that the performance of the turbine can be improved by applying a small amount of reaction in the rotors and the reversing vanes. These pressure drops accelerate the flows sufficiently to offset the decelerations from the frictional losses.

The turbine was originally designed with no reaction in the first rotor, 5% in the reversing row, and 4.3% in the second rotor.

Later in the program, the blades of the first rotor were rotated 2.1 degrees which decreased the flow area from 38.7-in.^{2} to 34.6-in.^{2}. This moved the zero reaction point from the blade mean line to the root to ensure a positive reaction at all times. It also ensured a downward thrust from the rotors in the exhaust direction at all of the engine operating points.

Appropriate turbine nomenclature is provided as Appendix A.

B. GAS PROPERTIES

The gas driving the turbine is the combustion product of liquid hydrogen and liquid oxygen. The effect of the pressure upon C_p and γ is neglected. Also, C_p and γ are taken at the inlet temperature of 1460°R. The gas properties used are as follows:

O/F	0.8	---
C_p	2.01	BTU/lbm-°R
γ	1.37	---
$\frac{\gamma - 1}{\gamma}$	0.27	---
$\frac{\gamma}{\gamma - 1}$	3.70	---
R	421.5	ft-lbf/lbm-°R

C. AERO-THERMODYNAMIC DESIGN

1. Loss Estimates

Two types of loss coefficients are used, one to determine the energy loss coefficient (ζ) from blade inlet to blade exit, the other to estimate the flow loss coefficient (ζ_a) from blade inlet to blade throat. The energy losses are used to determine stage and overall efficiencies while the flow losses are used to size the blade throat areas. The relationship between the two types of losses is discussed in Appendix B. Both loss coefficients for the nozzle are shown in Figure No. 3 and both loss coefficients for the rotors and the reversing vanes are shown in Figure No. 4. After-expansion losses are added to the nozzle and first rotor, both coefficients are corrected for the blade height. The velocity coefficients derived from the energy loss coefficients (ζ) for the turbine design point are as follows:

	Energy Loss Coefficient	Velocity Coefficient
Nozzle	0.120	0.9380
1st Rotor	0.277	0.8505
Reversing Row	0.169	0.9117
2nd Rotor	0.2135	0.8870

2. Performance

Based upon the loss estimation discussed in Paragraph III-C-1 of this report, the thermodynamic calculations of the rotor blades at the mean diameter were made and are summarized in Table II. From these data, the expansion process in the form of a temperature-entropy chart is shown as Figure No. 5. The velocity diagrams for the process are shown as Figure No. 6.

TABLE II

FLOW QUANTITIES AT THE TURBINE MEAN DIAMETER (23.0 IN.)

Parameter	Dimension	Nozzle Inlet	Nozzle Outlet	Rotor I Outlet	Reversing Vane Outlet	Rotor II Outlet
P_T	psia	1000	822.5	337.5	315.6	225.8
P_{TR}	psia	--	559.0	--	262.7	--
P_s	psia	--	250.0	250.0	230.0	214.0
T_T	°R	1460	1460	1226.1	1226.1	1133.4
T_{TR}	°R	--	1315.5	--	1167.02	--
T_s	°R	--	1058.5	1130.7	1125.9	1117.6
V	ft/sec	$\approx$ 0	6355.0	3099.5	3173.0	1283
U	ft/sec	--	1327	1327	1327	1327
W	ft/sec	--	5088.5	4310.0	2035.0	2228.0
α	degrees	$\approx$90	74.5	-61.25	66.0	-27.1
β	degrees	--	70.5	-69.75	50.15	-59.15
h_d	inch	--	1.48	1.73	2.24	2.62
Δ_b	inch	--	.410	.330	.380	--
M	--	--	1.433	.676	.694	.282
MR	--	--	1.147	.94	.445	.490

		Stage I	Stage II	Total
Lu	Btu/lbm	470	185	655
Li	Btu/lbm	454	173.5	627.5
η_i*	%	---	---	62.8
U/Co	--	---	---	0.196

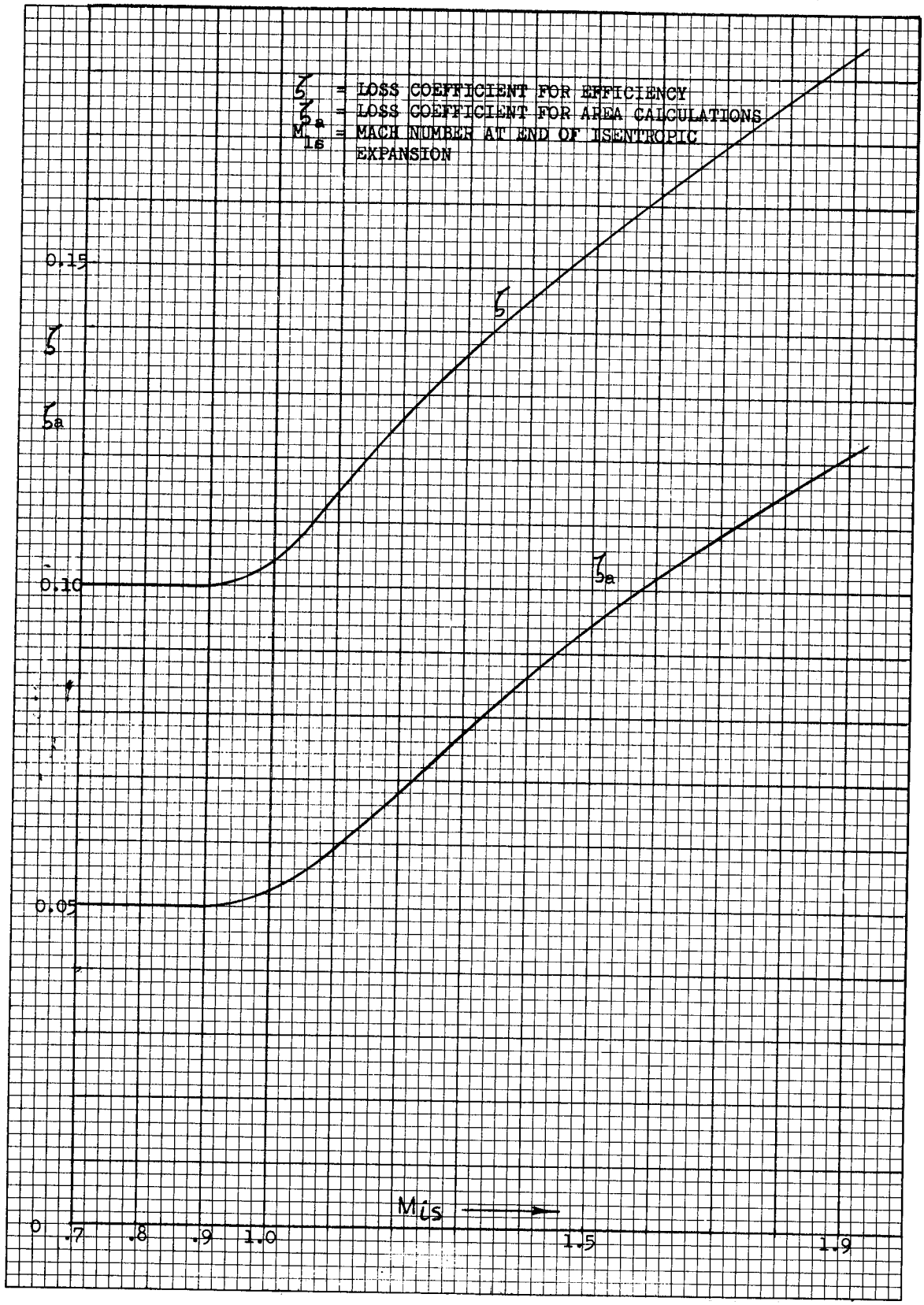

Figure 3. Loss Coefficients in Nozzles

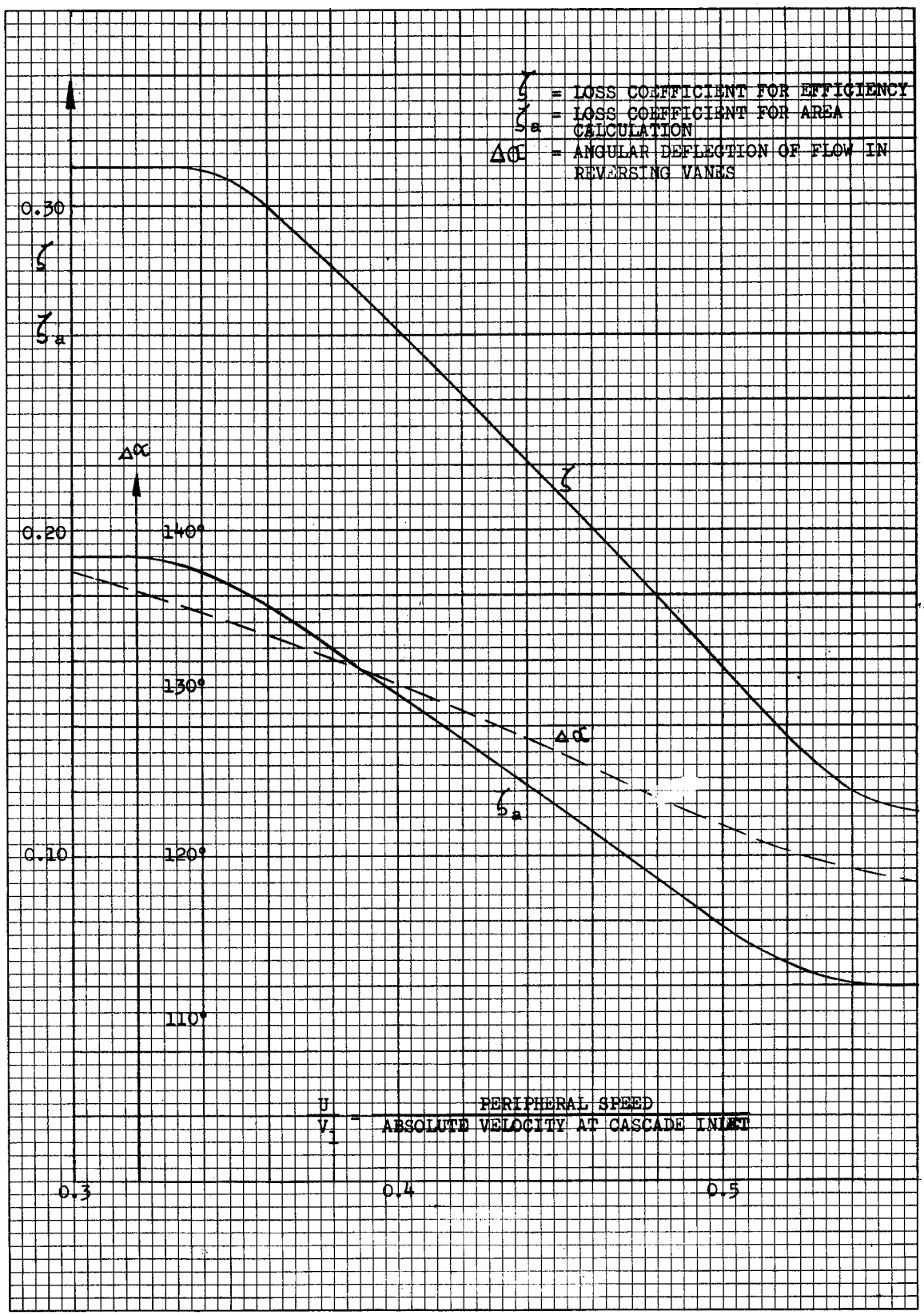

Figure 4. Loss Coefficients in Rotors and Reversing Vanes

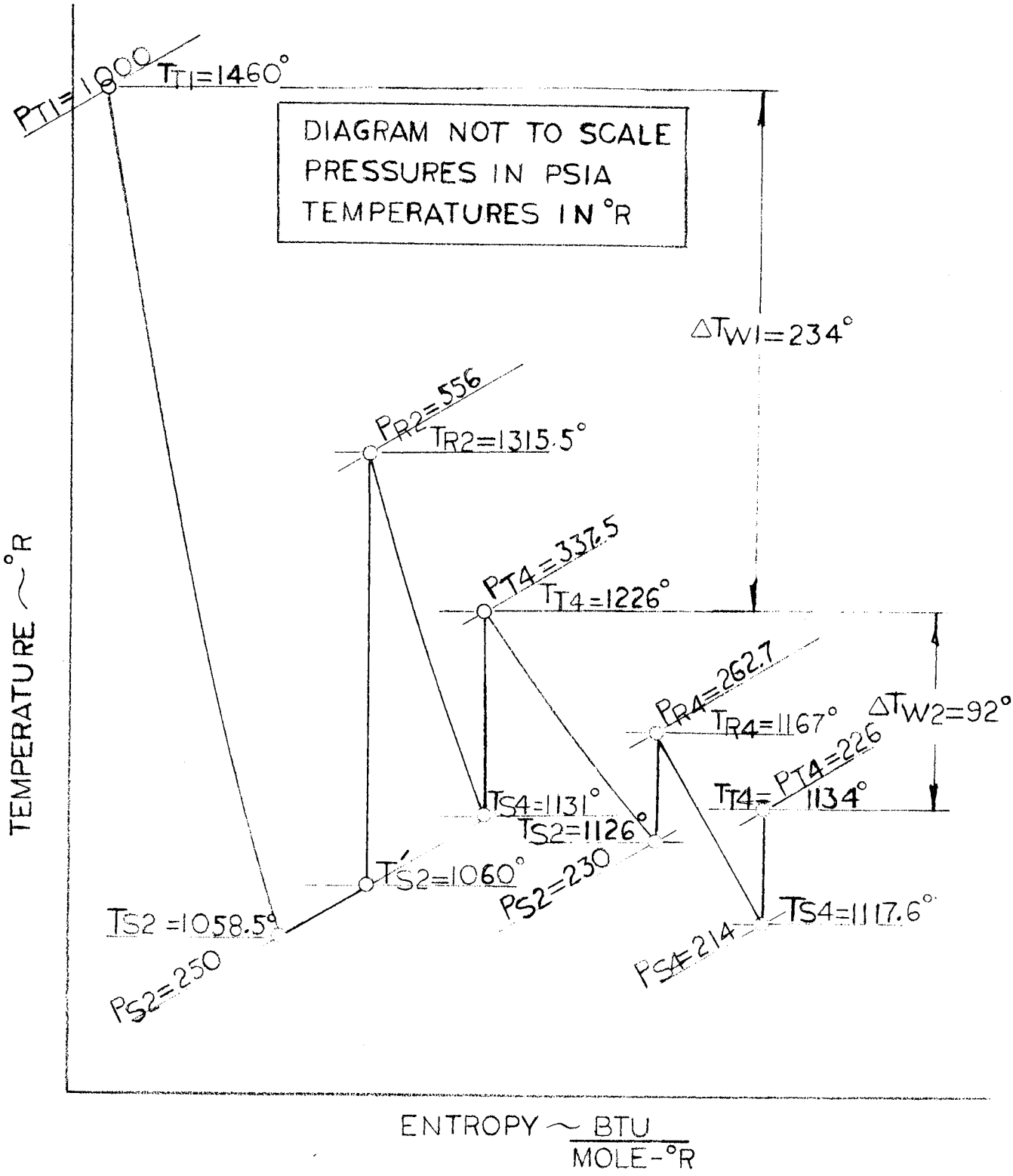

Figure 5. Temperature-Entropy Diagram

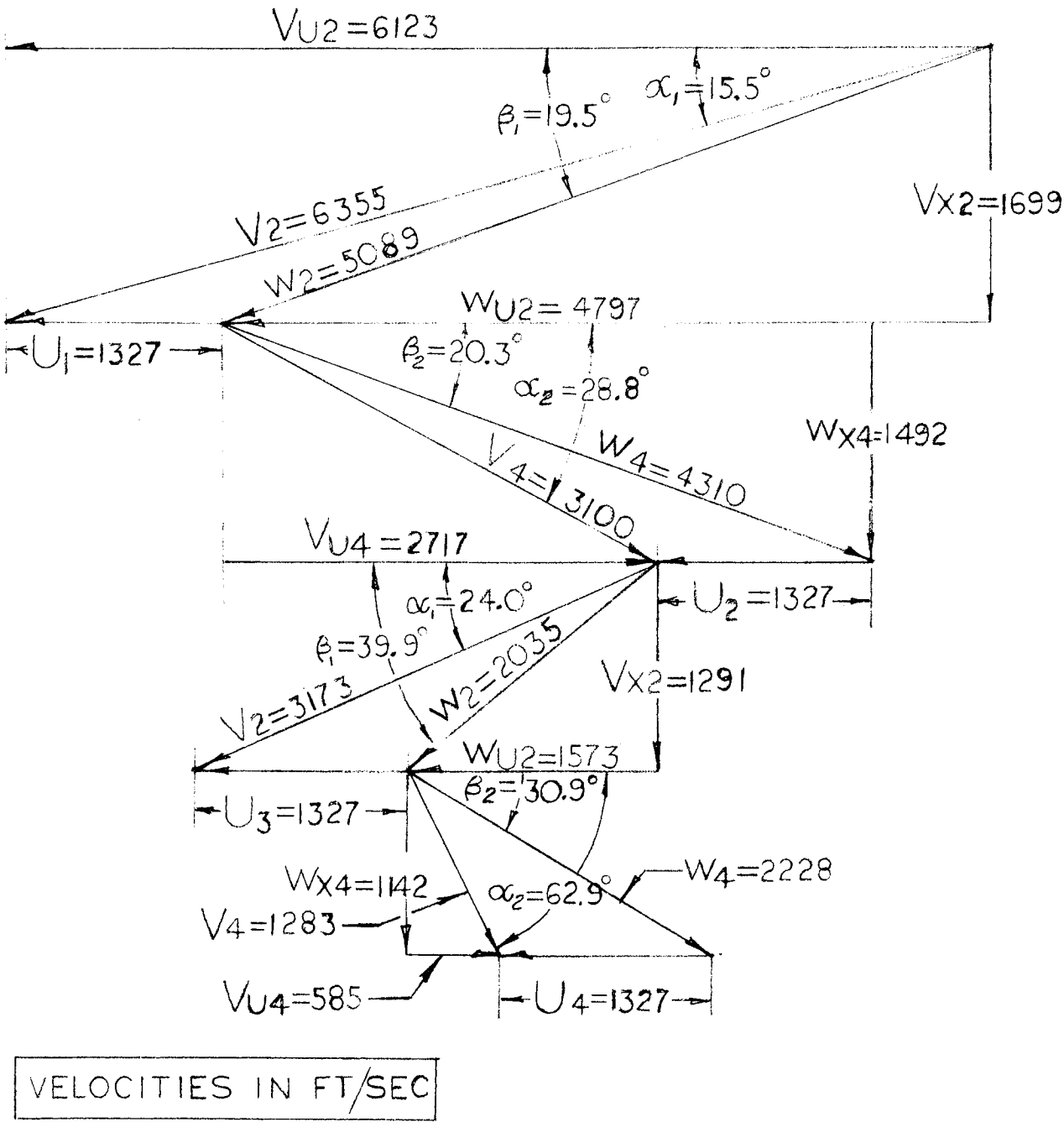

Figure 6. Velocity Diagram at Mean Blade Diameter

A total to static efficiency of 62.8% was obtained which included a leakage loss of 3.4% of the gas flow across the first rotor, 1.2% across the reversing row, and a 5.05% loss across the second rotor.

The predicted variation in turbine efficiency versus mean blade speed over spouting velocity (Um/Co) is shown in Figure No. 7.

D. CASCADE DESIGN

1. Supersonic Nozzle Design Considerations

As a general rule, it is of no advantage to install converging-diverging nozzles if the theoretical Mach number at the nozzle exit does not exceed about 1.2, or similarly, if the theoretical area ratio of the exit-to-throat is less than about 1.02.

Because the flow across the first-stage nozzle of this turbine has a pressure ratio of four, its theoretical Mach number is 1.575. Therefore, the nozzles should have divergent-convergent flow areas. Considerable after-expansions would occur if converging nozzles were used.(4) The critical pressure ratio for an isentropic expansion is 1.875. This would give an after expansion pressure ratio of 4/1.875 or 2.133. Using theoretical considerations, the above after expansion pressure ratio combined with a nozzle discharge angle of 75 degrees from the axial direction would cause a flow deflection of 3.5 degrees.(5) This would reduce the tangential velocity component by approximately 2%. Additional losses would occur from the entropy increase.

For these reasons, convergent-divergent nozzles with an area ratio that requires a slight after-expansion to obtain a pressure ratio of four are used. With a slight after-expansion, the nozzles become shorter and the frictional losses are reduced.

It was thought that supersonic nozzles should have a straight channel that does not change the direction of the flow after it leaves the throat.(6) The straight nozzles have long, thin walls at the discharge which are highly stressed.

Tests were made with a nozzle which is similar to, and has the same area ratio as the nozzle used for the M-1 fuel turbine.(7) These tests are discussed in detail in Appendix C where it is shown by the inclusion of a

(4) Howard, R. E., Jr., The Performance of High Power, Axial Flow, Turbine Utilizing Flows in the Transonic Regime, Master of Science Thesis, United States Naval Post Graduate School, Monterey, California, 1963.
(5) ibid.
(6) Markov, N. M., Calculation of the Aerodynamic Characteristics of Turbine Blading, Associated Technical Services Incorporated, Glen Ridge, New Jersey, 1958.
(7) Vavra, M. H., op. cit.

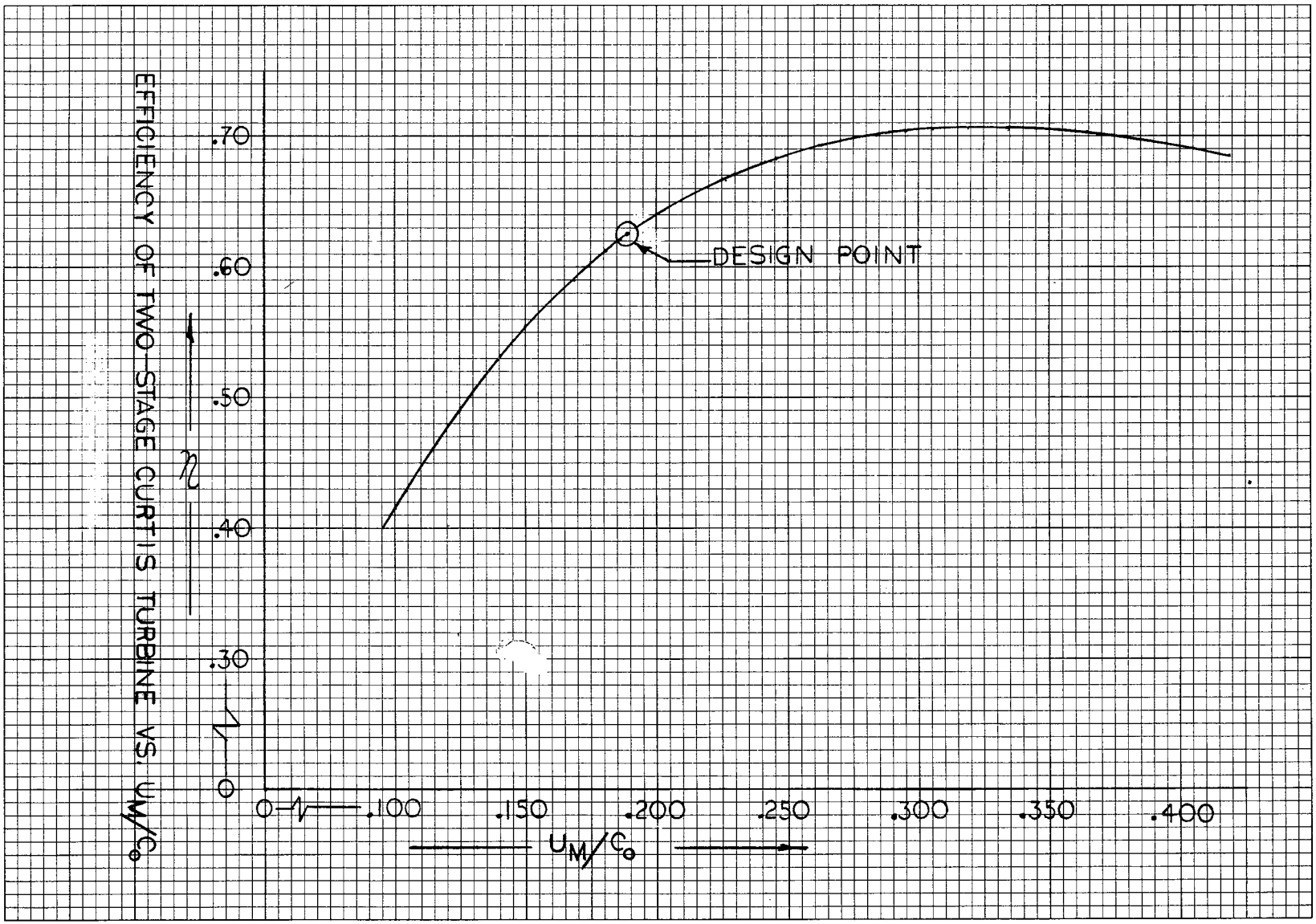

Figure 7. Efficiency of Two-Stage Curtis Turbine versus Um/Co

Schlieren photograph that no flow separations nor an excessive boundary layer buildup occur at a design point pressure ratio of four (Figure No. 4 of Appendix C). The effect of after expansion in the nozzles on the exit angle is clearly shown in another such photograph (Figure No. 5 of Appendix C).

It is apparent from looking at the nozzle profile (Figure No. 8) that curved nozzles are considerably stronger than straight nozzles. They do not have the long thin profiles which can easily be distorted by thermal and force effects. Curved nozzles also have the advantage of being easy to fabricate from light sheet metal. Therefore, curved nozzles were selected for the M-1 fuel turbine.

2. Blade Profiles and Solidities

It is usually advantageous to layout the different cascades with the smallest discharge angles that are possible. For the required discharge flow area, these angles are limited by the maximum blade heights that can be utilized, either because of the stress limitations, required overlaps, or the reasonable divergences of the meridional flow path. The flow path that was adapted represents a good compromise for a turbine having rotor blades with hub and tip diameters that are constant. The blade row heights and their axial positioning are shown in Figure No. 9.

The first-stage rotor blades have a supersonic relative velocity at the inlet. It has been shown through past experience with Curtis stages that rotor losses are not significantly increased unless the relative Mach number exceeds 1.2. However, the blade profile must have a thin and relatively sharp (.036-in.) leading edge, and the blade inlet angle must correspond closely with the gas inlet angle. Ideally, with small incidence angles, a normal shock will occur at the rotor inlet. This increases the entropy and decreases the effective total pressure ahead of the cascade.(8) The first rotor blade profile is shown in Figure No. 10.

The flow in the reversing vanes and the second rotor blades is subsonic. Their profiles have leading edges which are rounded to make them less sensitive to incidence angle changes. The gas discharge angles of the first and second rotor blades and of the reversing vanes are calculated in accordance with the following relationship.(9)

$$\sin \beta_2 = \frac{a}{s - t/\sin \beta_{2^*}}$$, where β_{2^*} is the blade angle. To this angle, the after-expansion deflection is added.(10)

(8) Vavra, M. H., Aero-Thermodynamics and Flow in Turbomachines, John Wiley and Sons, Incorporated, New York City, New York, 1960.
(9) Markov, N. M., op. cit.
(10) Vavra, M. H., Analysis and Design of the Modified 87-5 Turbine, AGTR No. 3 for Aerojet-General Corporation, April 1962.

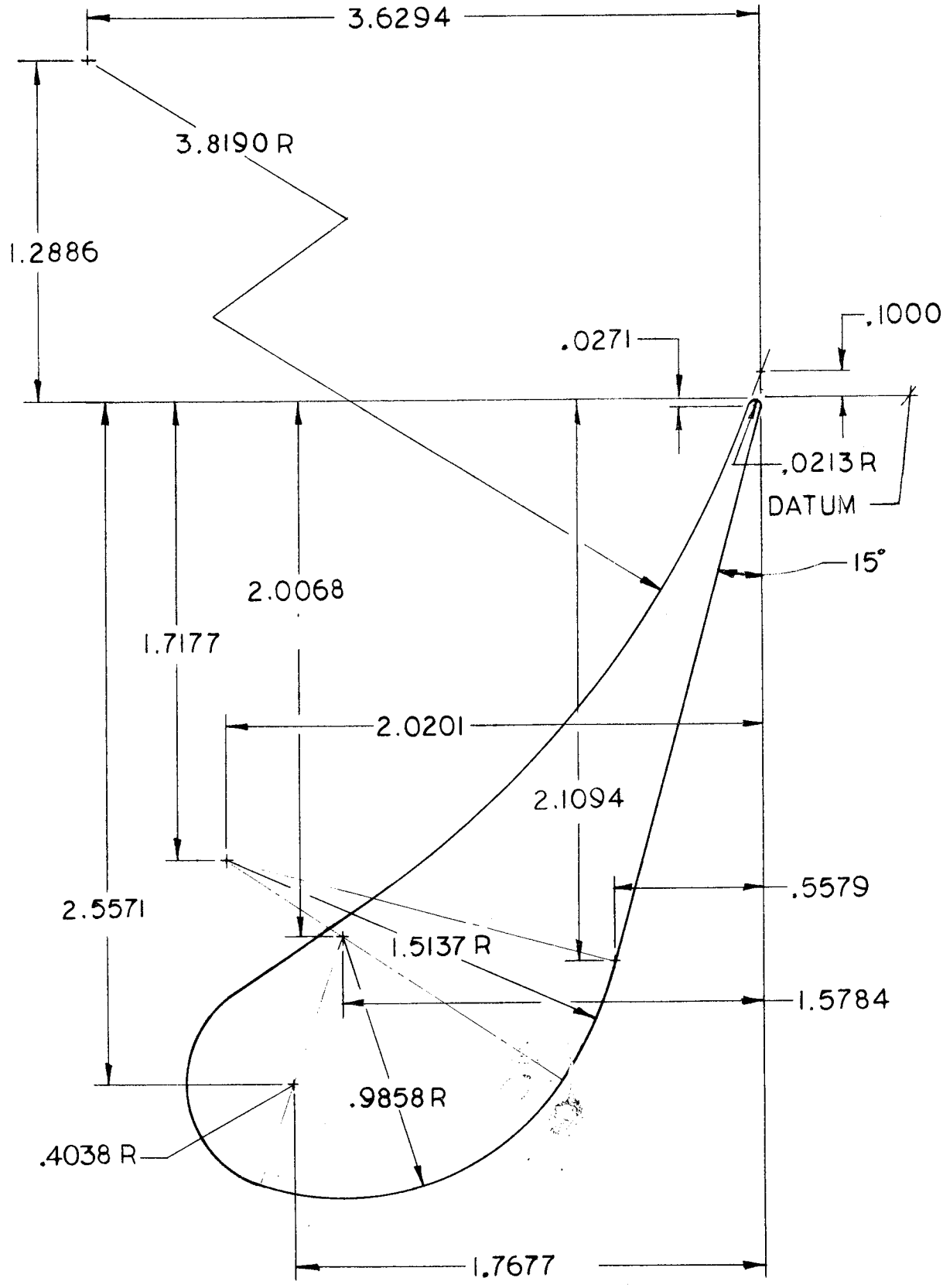

Figure 8. Nozzle Vane Profile and Dimensions

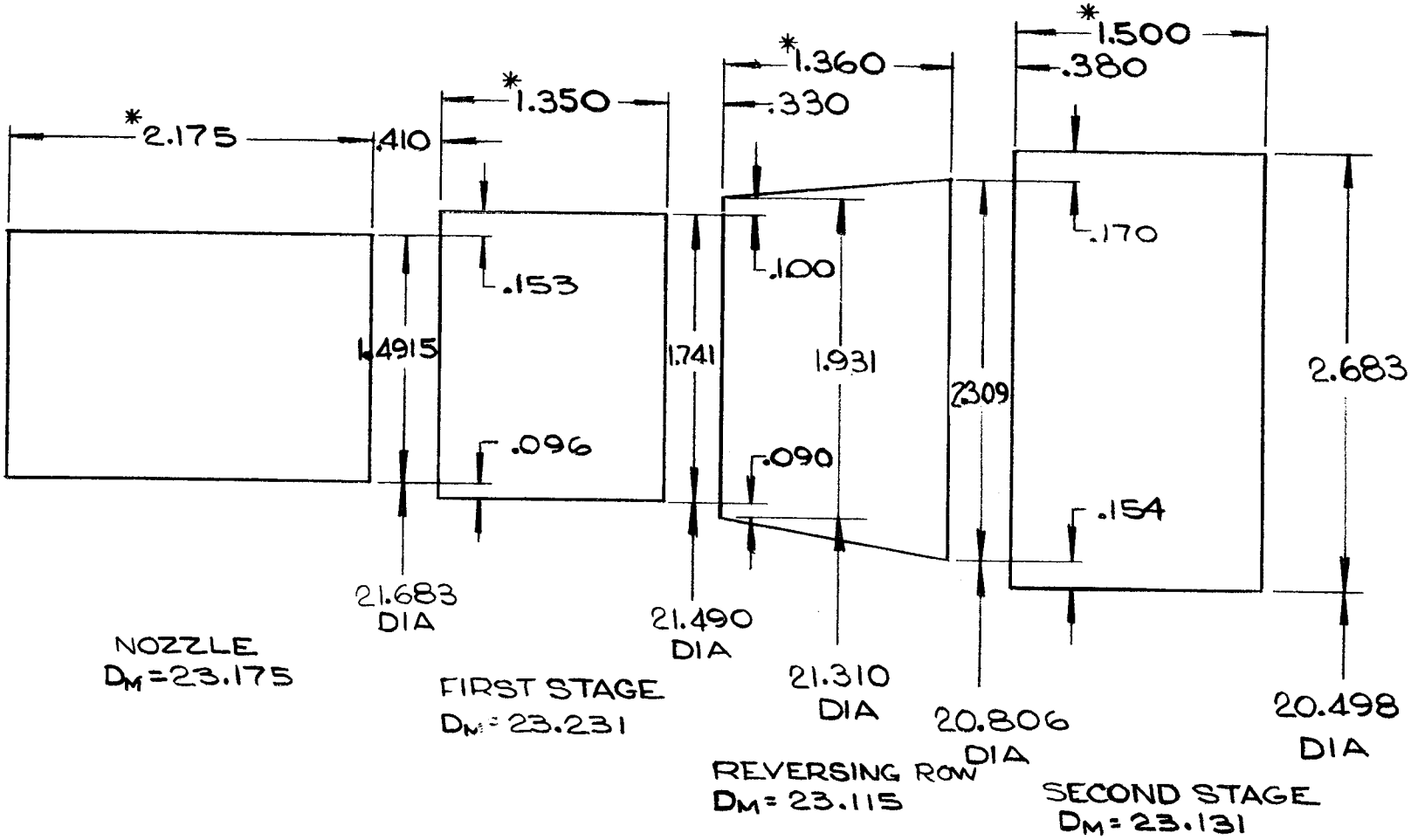

Figure 9. Axial Positioning of Blade Rows

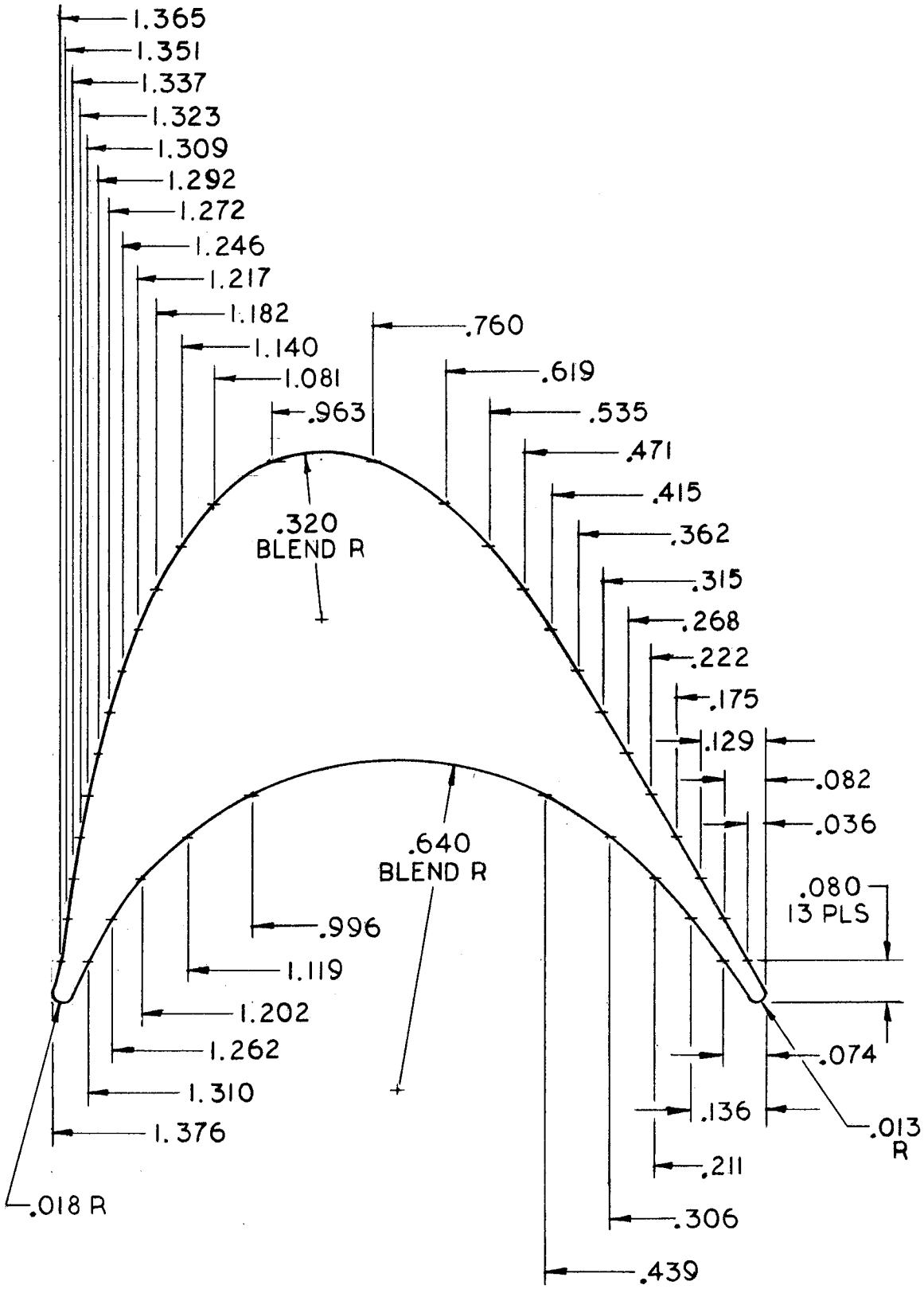

Figure 10. First Rotor Blade Profile and Coordinate

The profiles of the second rotor blades and the reversing vanes are shown in Figures No. 11 and No. 12.

The solidities of the blading selected for this design and the number of blades in each cascade are:

	Nozzle	First Rotor	Reversing Row	Second Row
Solidities	1.760	1.496	1.253	1.697
Number of Blades	37	80	67	78

The pitch, chord, and the stagger angle at the mean diameter of the blade are shown in the blading layout of Figure No. 13.

3. Flow Area Calculations

The determination of the correct flow areas is the most important step in the design of an efficient turbine. If these flow areas are wrong, the pressures downstream of the blade rows will differ from the assumed ones which will produce discharge velocities that differ from those used in the velocity diagram. This will cause the approach velocities of the following row of blades to have fluid angles that deviate from the blade angle design and this will reduce the performance of the turbine. Experience has shown that turbines usually have flow areas which are too large.

It is sometimes customary in the designing of turbines to introduce velocity coefficients that relate the actual discharge velocity of a row of blades to the isentropic velocity of the expansion process. These velocity coefficients are obtained by summing all of the losses that occur in the cascade. The coefficients include: the profile losses, the secondary losses, the mixing losses from flow wakes and trailing edges, the end losses, and the carryover loss from the exit of the flow from the preceding row of blades to the cascade under consideration. These velocity coefficients are also used to establish the density of the discharge gas by taking a loss coefficient of $1 - (\text{the velocity coefficient})^2$ for the total-to-static expansion process. The flow area is then determined from the density of the discharge gas which was derived and the velocity obtained by using the over-all velocity coefficient.

In the opinion of M. H. Vavra,[11] the losses from the cascade inlet-to-the-throat area at the cascade exit are considerably less than the losses obtained from using the over-all velocity coefficient of the cascade.

---

(11) Vavra, M. H., Aero-Thermodynamics and Flow in Turbomachines, John Wiley and Sons Incorporated, New York City, New York, 1960.

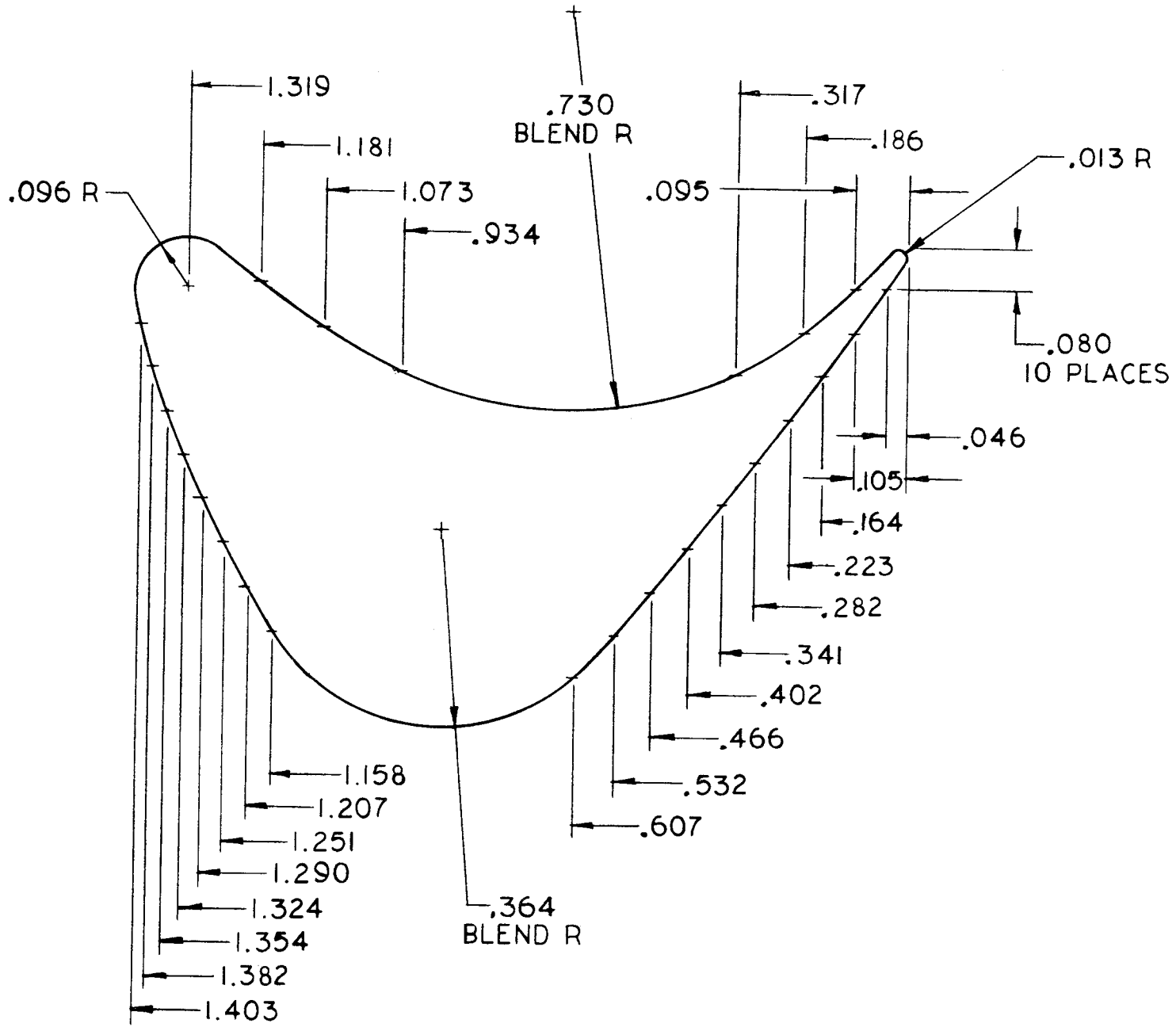

Figure 11. Reversing Vane Profile and Coordinates

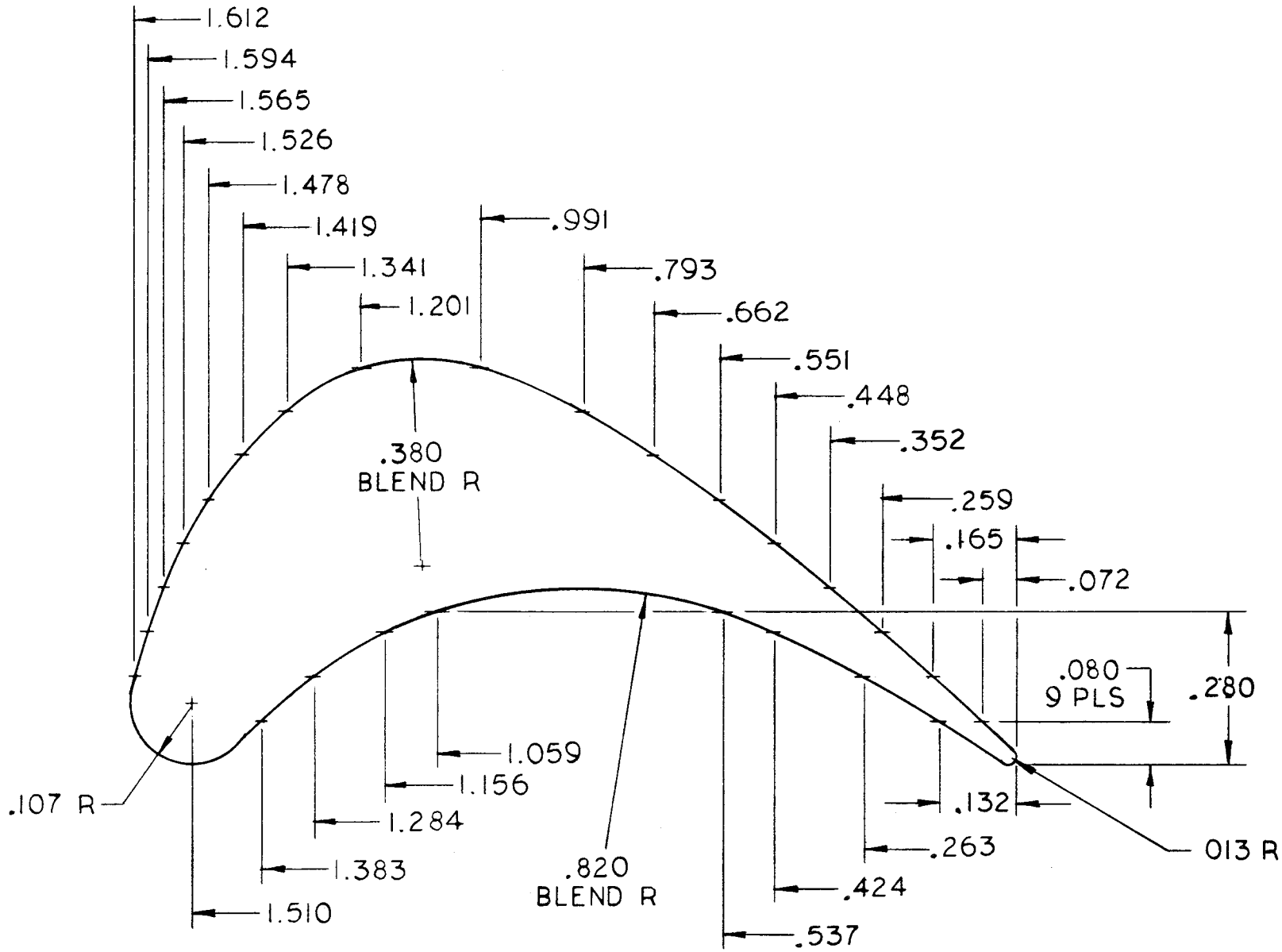

Figure 12. Second Rotor Blade Profile and Coordinates

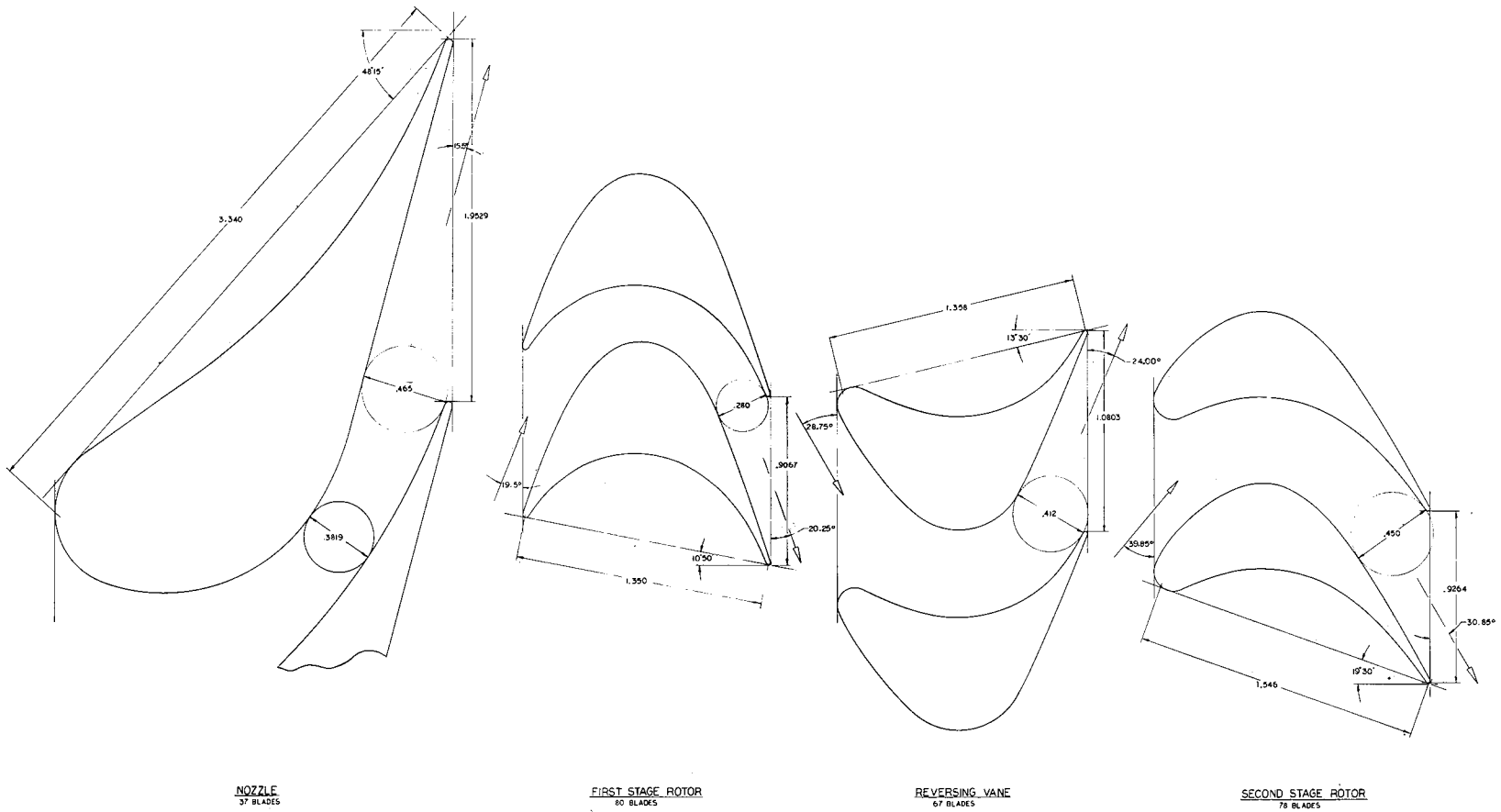

Figure 13. Blading Layout

The flow areas of the M-1 fuel turbine were calculated by the method shown in Appendix B. The equivalent loss coefficient for the nozzle is shown in Figure No. 3. The loss coefficients for the rotors and reversing vanes are shown in Figure No. 4. These are used in a polytropic expansion process. A dimensionless flow function ϕ^*, then is obtained which is defined by the equation

$$\phi^* = \frac{\overset{\circ}{M}\sqrt{T_T}}{P_T A}\sqrt{\frac{R}{g}} = \left\{ \frac{2\gamma}{\gamma-1}\left[\left(\frac{P_s}{P_T} \right)^{2/n} - \left(\frac{P_s}{P_T} \right)^{n+1/n} \right] \right\}^{1/2}$$

where the polytropic exponent n is

$$n = \frac{\gamma}{1 + \zeta_a (\gamma - 1)}$$

and where P_T and T_T represent the total pressure and the total temperature at the turbine nozzle entrance, and P_s is the static pressure at the nozzle exit.

The blade heights are corrected by the factors shown in Figure No. 14. The results of these calculations are shown in Table III.

4. Leakage Flow Calculations

The leakage flow through the axial clearances between the shrouds is calculated with a method developed by F. Salzmann.[12] This particular method is based upon theoretical findings that have been supported by model tests.

Different methods must be applied to determine the leakage between the nozzle and the first rotor than those used to determine the leakage between the first rotor and the reversing vanes (See Figure No. 15). For the leakage conditions shown in Figure No. 15a and the theoretical degree of reaction (R_x) of the stage, the ratio of the axial through flow velocity (V_{ml}), and the velocity (V^*) of the leakage flow at the clearance gap (k_a) are related by the following equation:

$$R_{xl} = \frac{1 - \left[1 - h_2^*/r_o \cot^2 \alpha_1 \right] (V_{ml}/V^*)^2}{1 + \left[1 - h_2^*/r_o \right] \cot^2 \alpha_1 (V_{ml}/V^*)^2}$$

This equation is also used to determine the leakage around the shroud of the second rotor.

---

(12) Salzmann, F., Veber Spaltverluste bei Dampf-Turbinenbes Chenfelungen, Escher-Wyss Mitteibugen, Volume III, No. 4/5, 1935.

TABLE III

DETERMINATION OF THROAT AREAS AND BLADE HEIGHTS*

		Nozzle	Rotor I	Reversing Vanes	Rotor II
T_T	°R	1460	1315.5	1226.1	1167.0
P_T	psia	1000	556	337.5	262.7
P_s	psia	267	305	230	214
ϕ^* to Throat	---	0.6594	---	---	---
ϕ^* to Discharge	---	0.5280	0.6066	0.6053	0.5090
ζ_a to Throat	---	0.0435	---	---	---
ζ_a to Discharge	---	0.0785	0.1575	0.1009	0.1130
Throat Area	$in.^2$	20.91	38.7**	61.83	91.96
Number of Blades	---	37	80	67	78
Throat Width	in.	0.3819	0.280**	0.412	0.450
Blade Height, h	in.	1.480	1.730	2.240	2.620

---

* Dimensions are for components at 68°F and zero rpm.

** Rotating the first rotor blading by 2.1-degrees resulted in a throat width of 0.250-in. and a throat area of 34.6-in.^2.

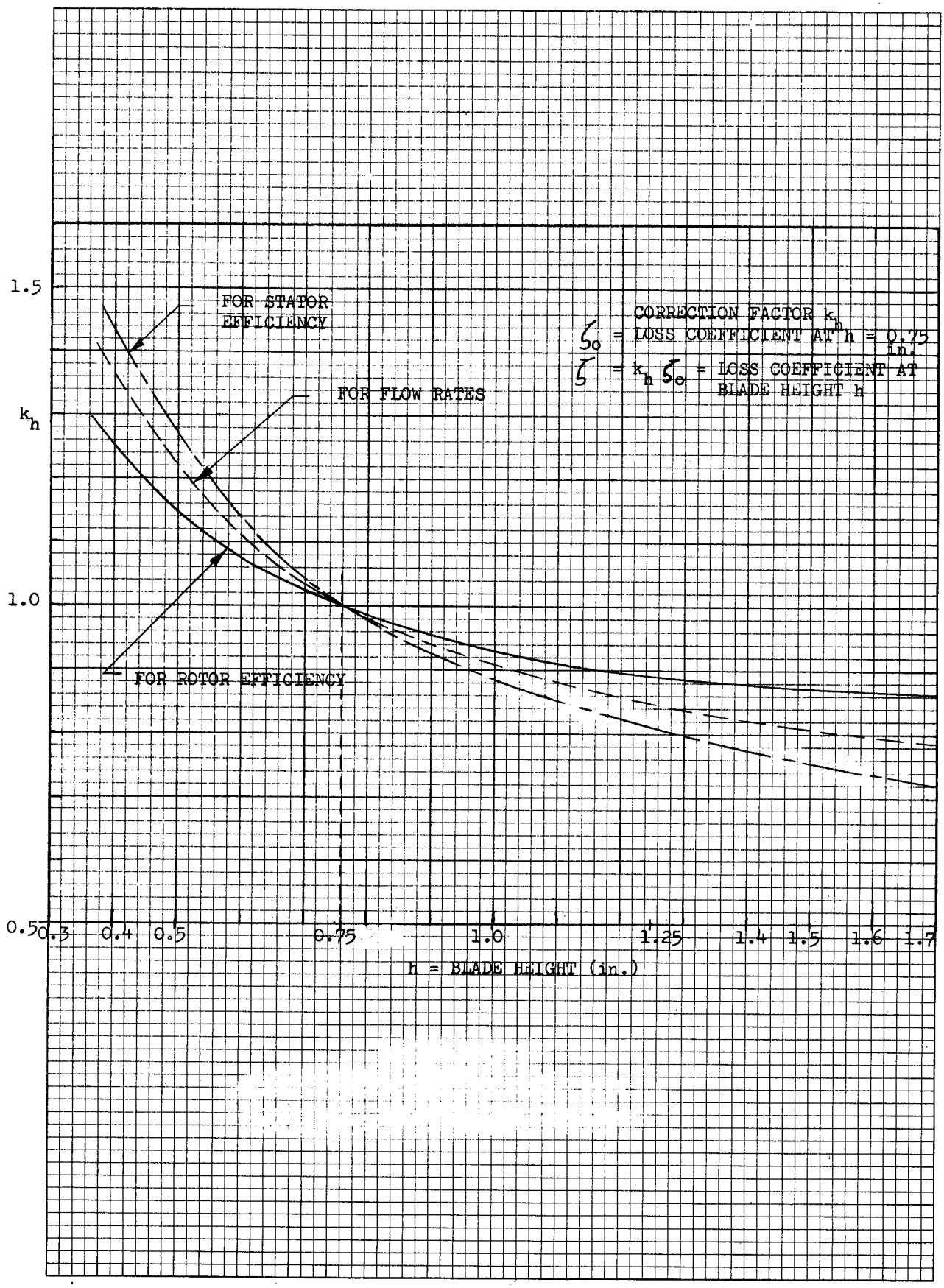

Figure 14. Effect of Blade Height on Loss Coefficients

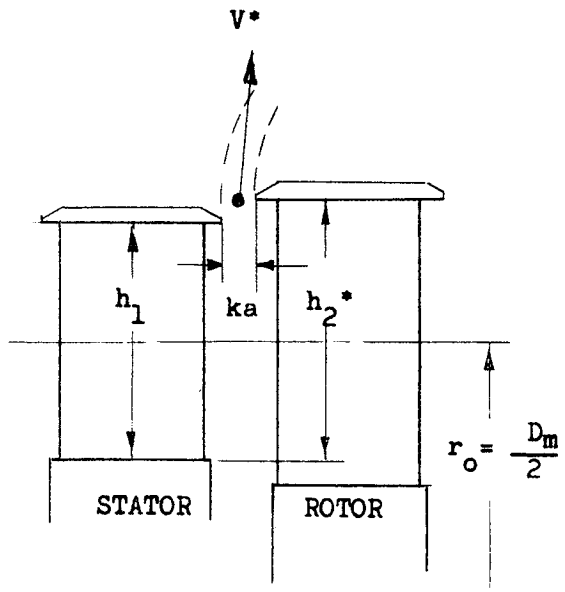

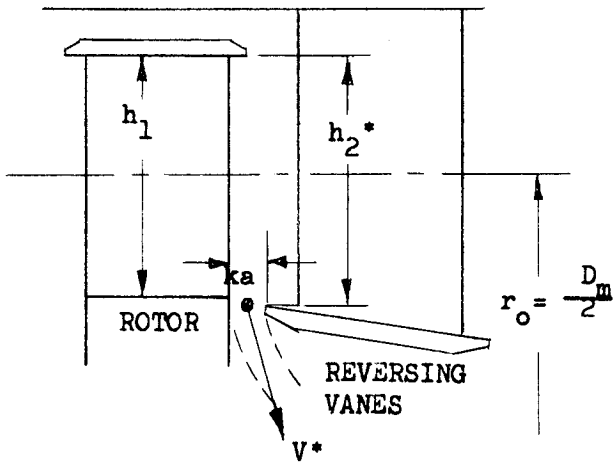

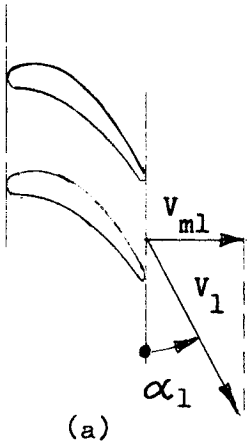

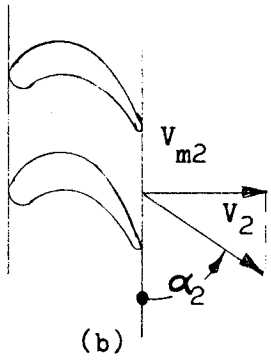

α_1 = ANGLE OF ABSOLUTE VELOCITY V_1

AROUND SHROUD OF ROTOR BLADES

α_2 = ANGLE OF ABSOLUTE VELOCITY V_2

AROUND INNER SHROUD OF REVERSING VANES

Figure 15. Symbols and Conditions for Leakage Flow Calculations

To determine the leakage across the inner shroud of the reversing vanes, Figure 15b is used with the following equation:

$$R_{x2} = \frac{1 + \left[h_2^*/r_o \cot^2 \alpha_2 - 1 \right] (V_{m2}/V^*)^2}{1 + \left[1 + h_2^*/r_o \right] \cot^2 \alpha_2 (V_{m2}/V^*)^2}$$

The degree of reaction (Rx_1) is the ratio of the static isentropic enthalpy drop in the rotor and the total to static isentropic enthalpy drop of the whole stage.

The degree of reaction (Rx_2) is the ratio of the static isentropic enthalpy drops in the reversing vanes and that from the total pressure ahead of and the static pressure downstream of the reversing vanes.

After V_{m1}/V^* and V_{m2}/V^* are determined from the preceeding equations, the leakage flow coefficients (ζ_L) can be determined using Figure 16 for the different ratios of k_a/h_1 and h_2/h_1. Depending on the sealing arrangement, a certain leakage restriction factor (k_L) is applied to obtain the actual leakage flow. For this application, the leakage restriction factor between nozzles and the first rotor is taken as 0.85, for the reversing vanes inner shroud the factor is 0.75, and for the second rotor a factor of 0.95.

The actual power output of the turbine becomes

$$HP_e = (1 - \zeta L_1) HP_I + (1 - \zeta L_R - \zeta L_2) HP_{II}$$

where HP_I and HP_{II} are the power outputs of the first and second rotors. The results of the leakage flow calculations are summarized in Table IV. The leakage flow coefficients are shown on Figure No. 16.

5. Velocity Distribution on Blade Profiles

The National Aeronautics and Space Administration computer program[13] was used to estimate the velocity distribution on the profiles. The degree of accuracy which can be achieved with this method depends upon the accuracy of the computer input data. It is difficult to estimate the effective channel at the inlet to the blades. As a result dashed lines are used to show the probable values of velocity distribution during the first few percentages of the blade width.

(13) Stinson, W. D., Turbine Computer Program, NASA-Aerojet Computer Job No. 1009, Aerojet-General Corporation Memorandum, dated 27 September 1962.

TABLE IV

SUMMARY OF LEAKAGE FLOW CALCULATIONS

Parameter	Rotor 1	Reversing Vanes	Rotor 2
h_1	1.480	1.730	2.240
h_2^*	1.650	1.820	2.390
α_1, α_2	15.0°	28.75°	24.0°
k_a	0.12	0.125	0.135
k_a/h_1	0.081	0.073	0.061
Rx	0	0.209	0.149
V_{m1}/V^* and/or V_{m2}/V^*	0.596	0.778	0.487
ζ_L (Figure 14)	4.0%	1.5%	5.6%
k_L	0.85	0.75	0.90
$\zeta_L k_L$	3.4%	1.2%	5.05%

Symbols are the same as those used in Figure No. 15 and No. 16.

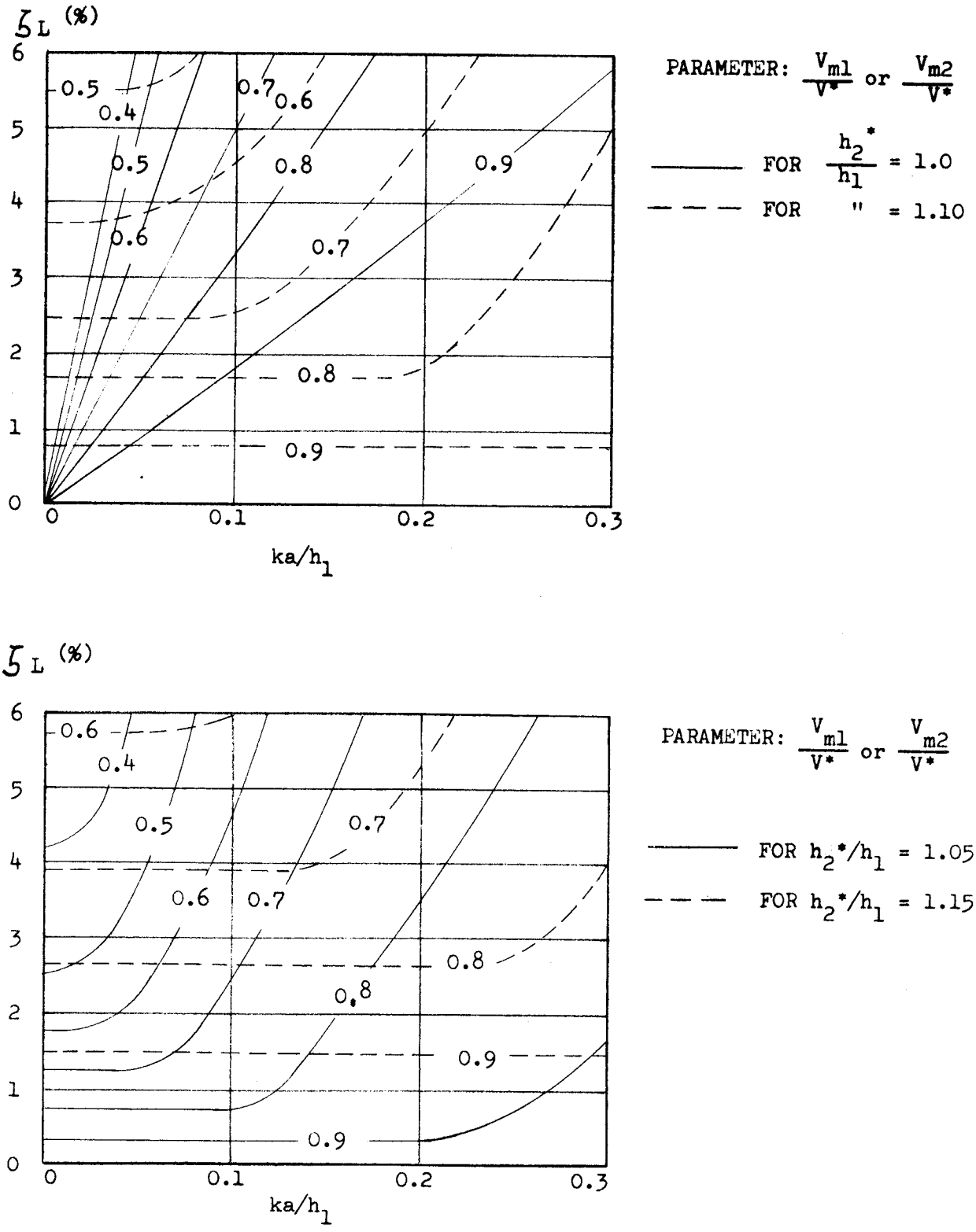

Figure 16. Leakage Flow Coefficients

The design point velocity distributions are shown in the following figures:

Nozzle	Figure No. 17
First Rotor	Figure No. 18
Reversing Row	Figure No. 19
Second Rotor	Figure No. 20

The nozzle velocity distribution shown in Figure 17 indicates that the selected profile is adequate.

The velocity distribution of the first rotor blades is shown in Figure 18. Considerable diffusion is apparent, particularly at the root and mean pressure surface. The profile seems to be satisfactory.

The second stator or reversing row velocity distribution as shown by Figure 19 indicates that the profile is satisfactory.

The velocity distribution of the second rotor (Figure 20) looks very satisfactory.

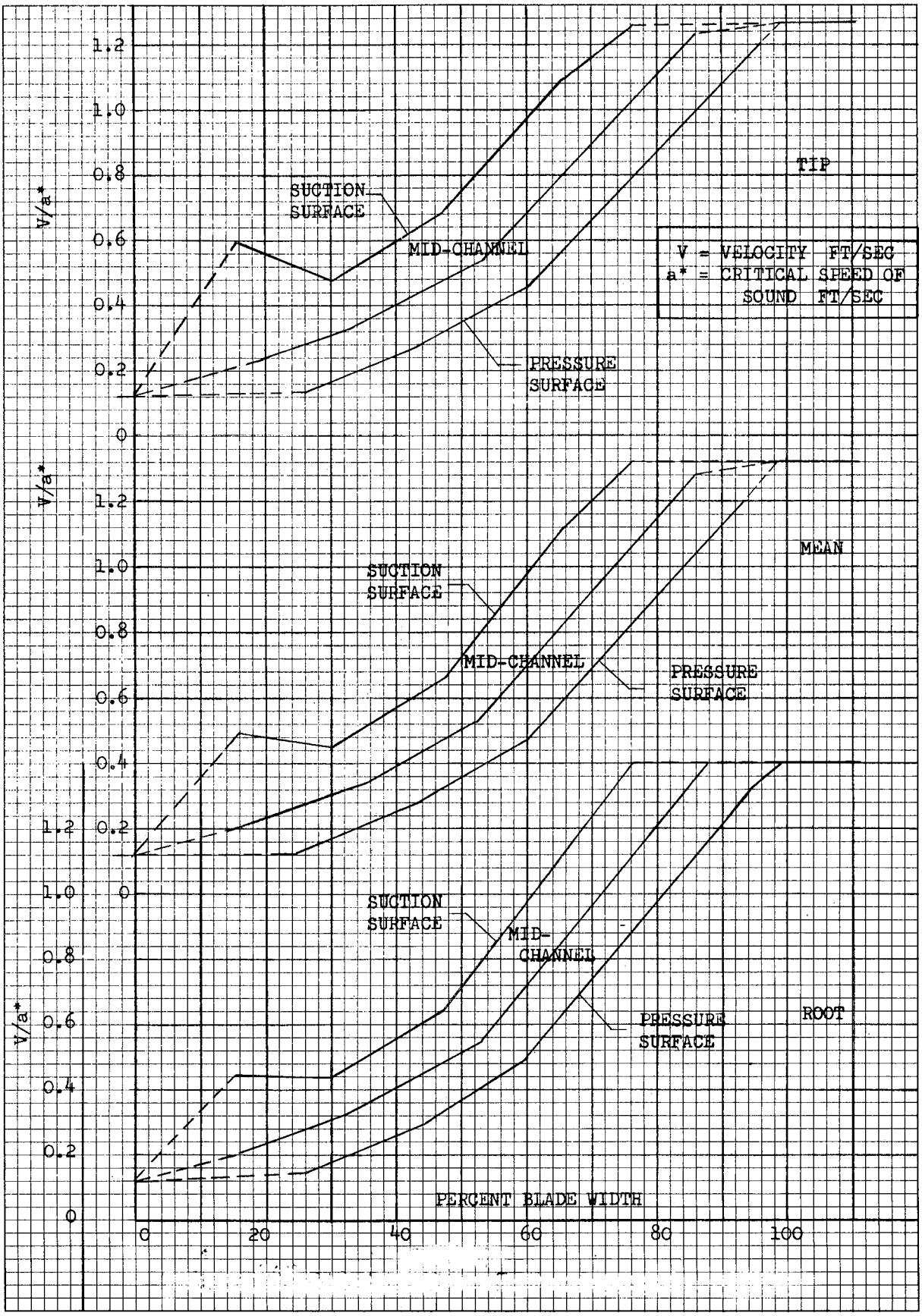

Figure 17. Velocity Distribution for the Nozzle, 37 Vanes

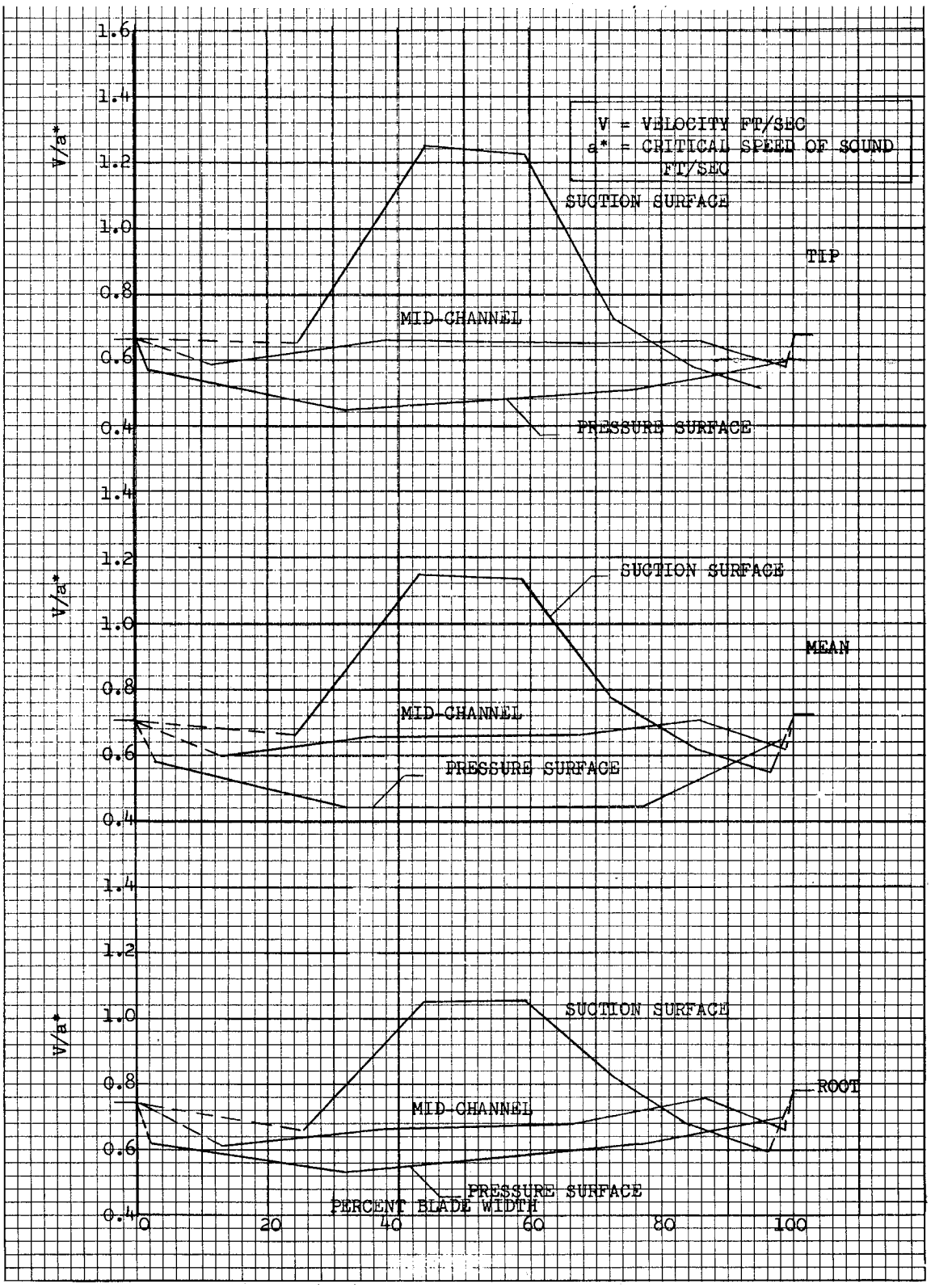

Figure 19. Velocity Distribution for the Reversing Row, 67 Vanes

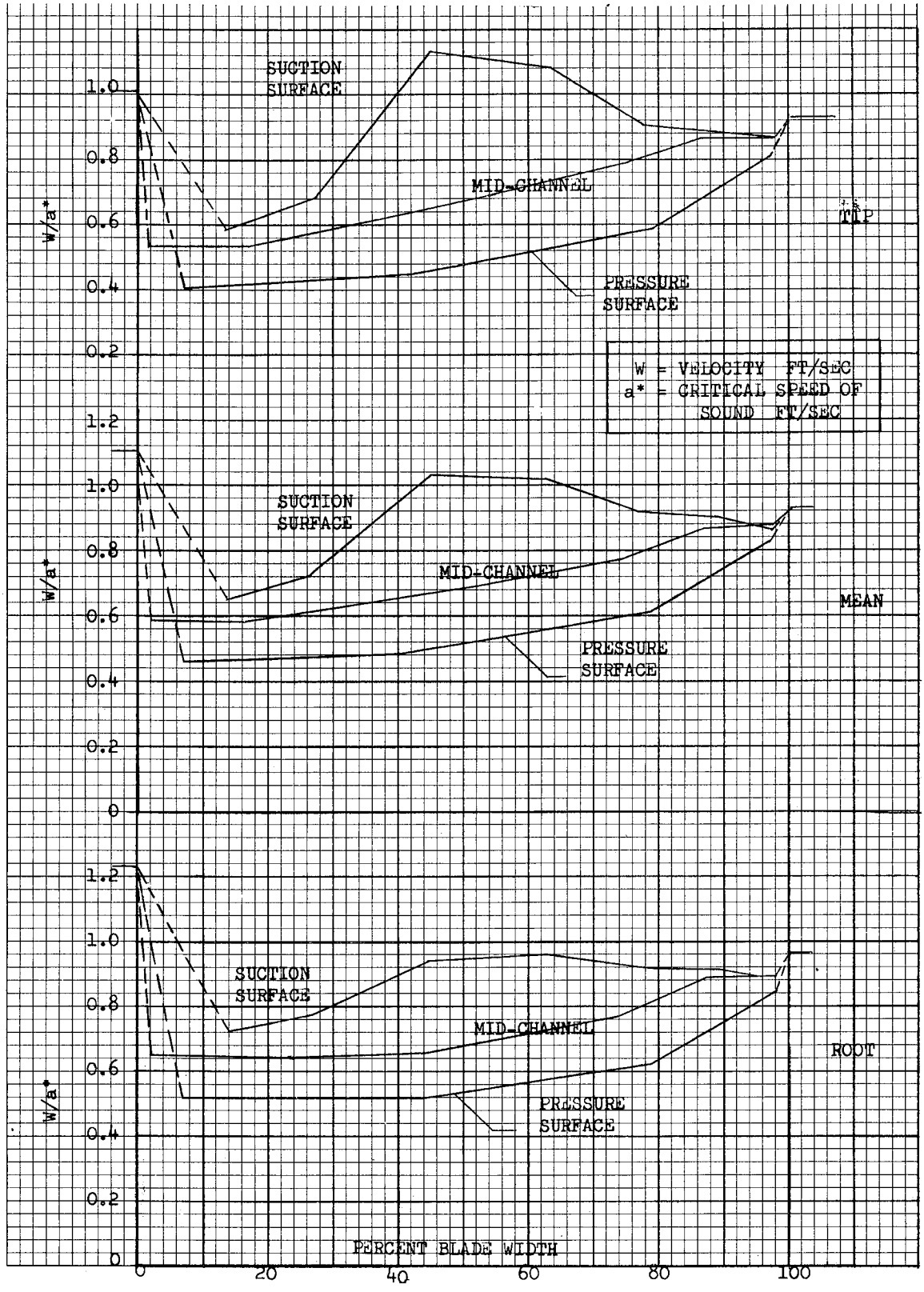

Figure 18. Velocity Distribution for the First Rotor, 80 Blades

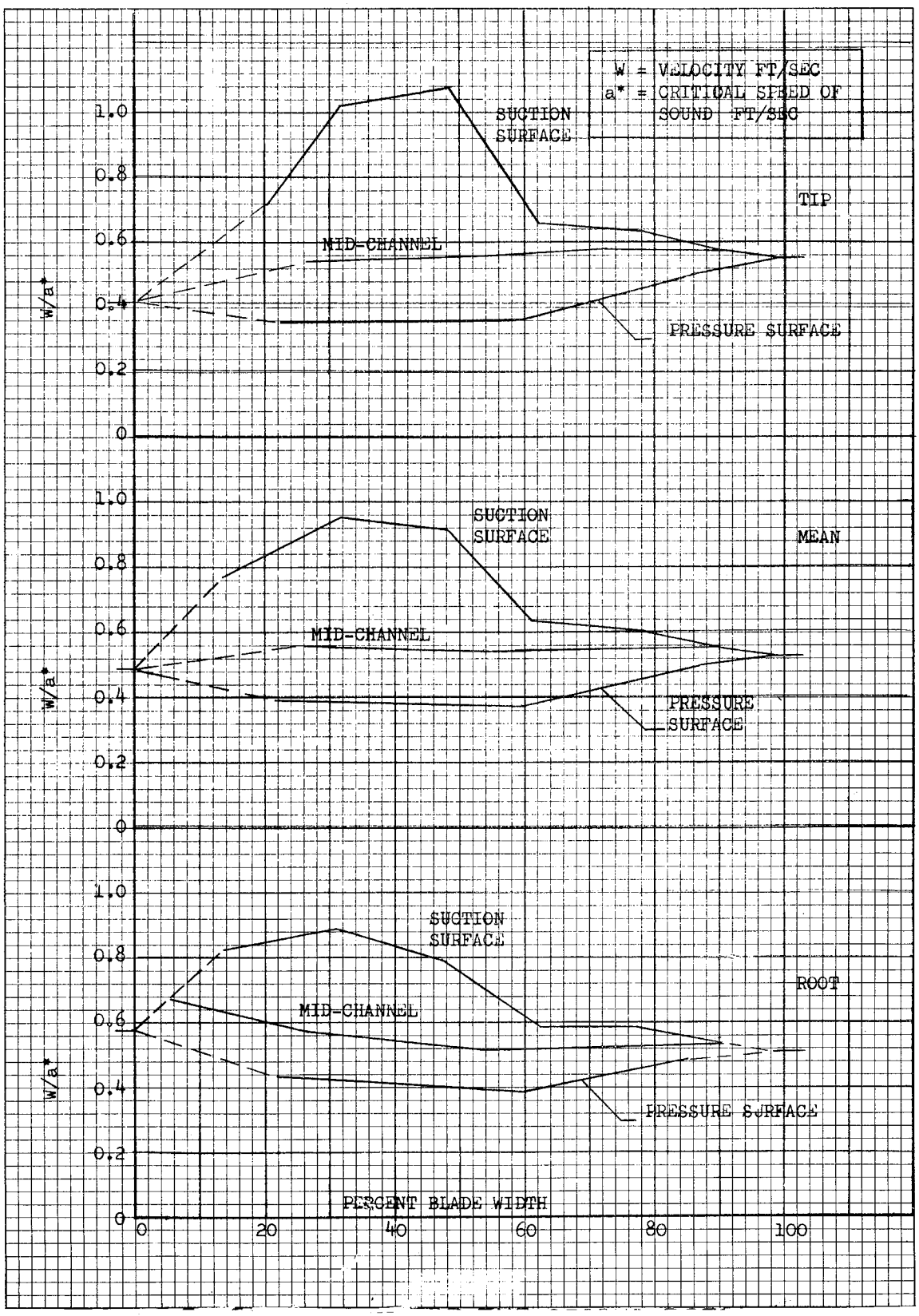

Figure 20. Velocity Distribution for the Second Rotor, 78 Blades

BIBLIOGRAPHY

1. Howard, R. E., Jr., The Performance of High Power, Axial Flow, Turbines Utilizing Flows in the Transonic Regime, Master of Science Thesis, United States Naval Post Graduate School, Monterey, California, 1963

2. Markov, N. M., Calculation of the Aerodynamic Characteristics of Turbine Blading, Associated Technical Services Inc., Glen Ridge, New Jersey, 1958

3. Reynolds, T. W., The Mechanical Design of a Two-Stage Impulse Turbine for the Liquid Hydrogen Turbopump of the M-1 Engine, NASA Report CR-54821, 22 April 1966 (Aerojet-General Corporation Report No. 8800-58)

4. Salzmann, F., Ueber Spaltverluste bei Dampf-Turbinenbeschaufelungen, Escher-Wyss Mitteilungen, Vol. VIII, No. 4/5, 1935

5. Stinson, W. D., Turbine Computer Program, NASA-Aerojet Computer Job No. 1009, Aerojet-General Corporation, Memorandum, dated 27 September 1962

6. Vavra, M. H., Aero Thermodynamics and Flow in Turbomachines, John Wiley & Sons, Inc., New York City, New York, 1960

7. Vavra, M. H., Analysis and Design of Modified 87-5 Turbine, AGR No. 3 for Aerojet-General Corporation, April 1962

8. Vavra, M. H., M-1 Fuel Turbine, Aerodynamic Design, AGR No. 0143, Aerojet-General Corporation, November 1963

APPENDICES

APPENDIX A

TURBINE NOMENCLATURE

TURBINE NOMENCLATURE

SYMBOL	DESCRIPTION	UNITS
a	Local Speed of Sound, $a^2 = \gamma g R T_s$	Ft/Sec
a*	Critical Speed of Sound, $a^{*2} = \frac{2\gamma}{\gamma+1} g R T_T$	Ft/Sec
A	Area	In^2
b	Axial Blade Width	Inch
Δb	Axial Distance Between Blade Rows	Inch
c	Blade Chord	Inch
C_o	Isentropic Velocity, $C_o^2 = 2gJ \Delta H'$	Ft/Sec
C_P	Specific Heat at Constant Pressure	Btu/Lb-°R
C_v	Specific Heat at Constant Volume	Btu/Lb-°R
d	Throat Width	Inch
D	Diameter	Inch
g	Acceleration Due to Gravity (32.17)	Ft/Sec^2
h	Blade Height	Inch
H	Specific Total Enthalpy	Btu/Lb
i	Incidence	Degrees
J	Mechanical Equivalent of Heat (778.2)	Ft Lb/Btu
K_R	Rotor Velocity Coefficient, W_L/W_4'	-----
k_a	Axial Clearance	Inch
k_n	Height Correction Factor	-----
k_L	Leakage Correction Factor	-----
L_u	Specific Work in Blading	Btu/Lbm
L_i	Specific Internal Work	Btu/Lbm
M	Absolute Mach Number	-----

SYMBOL	DESCRIPTION	UNITS
M_R	Mach Number Relative to Rotor Blade	----
$\dot{m}$	Mass Flow	Lbm/Sec
m	Exponent of Power Profile of Boundary Layer	----
n	Polytropic Exponent	----
N	Rotational Speed	RPM
P_s	Static Pressure	psia
P_T	Total Pressure	psia
P_{TR}	Total Pressure Relative to Rotor Blade	psia
q	Dynamic Head, $1/2 \quad \frac{\rho V^2}{144g}$	psi
R	Gas Constant	$\frac{\text{Lbf-Ft}}{\text{Lbm-}^\circ\text{R}}$
r	Radius	Inch
R_x	Degree of Reaction: $R_x = \frac{T_{s2'} - T_{s4'}}{T_{T1} - T_{s4'}}$	----
s	Blade Pitch	Inch
t	Maximum Blade Thickness	Inch
t_e	Trailing Edge Thickness	Inch
T_T	Total Temperature	$^\circ$R
T_s	Static Temperature	$^\circ$R
T_{TR}	Total Temperature Relative to Rotor Blade	$^\circ$R
U	Wheel Speed	Ft/Sec
u	Velocity in Boundary Layer	Ft/Sec
V	Absolute Velocity	Ft/Sec
W	Velocity Relative to Rotor	Ft/Sec
y	Distance in Boundary Layer	Inch
α	Angle Between Axial Direction and Absolute Gas Velocity	Degrees

SYMBOL	DESCRIPTION	UNITS
β	Angle Between Axial Direction and Relative Gas Velocity	Degrees
β *	Blade Angle	Degrees
γ	Gas Specific Heat Ratio, Cp/Cv	----
δ	Boundary Layer Thickness	Inch
δ *	Displacement Thickness of Boundary Layer	Inch
δ ***	Energy Thickness of Boundary Layer	Inch
Δ	Prefix to Indicate Change	----
ζ	Loss Coefficient for Efficiency	----
ζ_a	Loss Coefficient for Area Calculation	----
ζ_L	Leakage Loss	
Z	Stagger Angle	Degrees
η_T	Turbine Efficiency Based on Total to Static Pressure Ratio	%
η_i*	Internal Efficiency, Total to Static	%
θ	Camber Angle	Degrees
λ	Work-Speed Parameter = $U_m^2/gJ\Delta H$	----
	Velocity Ratio = U_m/C_o	----
ρ /g	Specific Mass	Lb-Sec^{2}Ft^4
ρ	Specific Weight or Density	Lb/Ft^3
σ	Blade Solidity = c/s	----
τ	Radial Tip Clearance	Inch
Ψ	Restriction Factor	----
φ	Blade Angle from Axial Direction	Degrees
ϕ *	Flow Function	----
ω	Angular Velocity	Rad/Sec

SUBSCRIPTS

1	Inlet to Stator
2	Outlet of Stator
3	Inlet to Rotor
4	Outlet of Rotor
D	Design Point
d	Blade or Throat Discharge
h	At Blade Root
i	Internal
M	At Mean Blade Height
R	Relative
S	Static
t	At Blade Tip
u	Tangential Component
x	Axial Component

Superscripts

' (Hyphen)	For Temperature or Enthalpy, Means Isentropic Expansion

DEFINITIONS

Camber Line	Locus of the Centers of Circles Described Inside the Blade Contour
Camber Angle, θ	The Angle Between Tangents to the Camber Line in Leading Edge and Trailing Edge
Chord Line	Line Connecting the Leading Edge and the Trailing Edge of the Camberline
Chord, c	Linear Distance in Inches Between Leading Edge, and Trailing Edge
Blade Inlet Angle	The Angle Between the Tangent of the Camberline in its Leading Edge and the Turbine Axis
Blade Outlet Angle	The Angle Between the Tangent of the Camberline in its Trailing Edge and the Turbine Axis
Stagger Angle, Z	The Angle Between the Chord Line and the Turbine Axis
Incidence, i	The Angle Between the Tangent of the Camberline in its Leading Edge and the Direction of the Undisturbed Flow Upstream of the Blade
Deviation, δ	The Angle Between the Tangent of the Camberline in its Trailing Edge and the Direction of the Airflow Downstream of the Blade
Pitch, s	Distance Between Corresponding Points on Adjacent Blades
Solidity, σ	Chord/Pitch

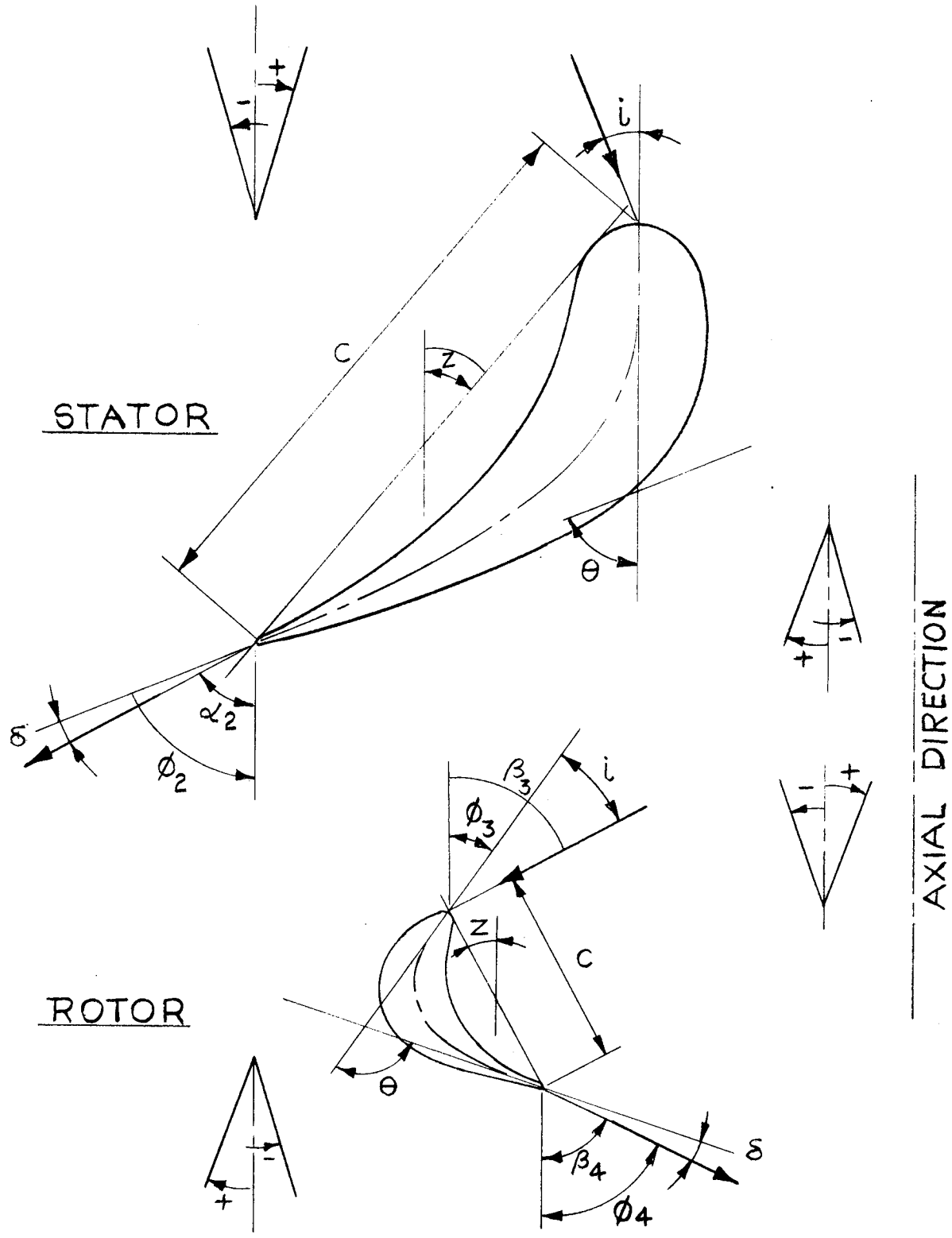

FIGURE A-1

BLADE NOMENCLATURE AND SIGN CONVENTION

APPENDIX B

BOUNDARY LAYER EFFECT ON FLOW RATES THROUGH CASCADES

BOUNDARY LAYER EFFECT ON FLOW RATES THROUGH CASCADES[1]

I. ESTABLISHMENT OF THE FLOW AREA LOSS COEFFICIENT

An investigation of the boundary layer conditions at the throat was used to determine the throat areas for the M-1 turbine. The displacement thickness of the throat boundary layers can be related to the profile losses which, in turn, depend upon the energy thickness of the boundary layer. Compressibility effects in the boundary layer can also be accounted for by the change in density (ρ). It is then possible to establish an equivalent loss coefficient for the area calculation which can be used in a polytropic expansion process.

II. MASS FLOW RATE AT DISCHARGE

Figure B-1 of this Appendix shows the flow conditions that occur at the discharge of a cascade in relationship to the boundary layers that have been formed on both sides of the profiles. With non-separated flows, the velocity outside the boundary layers is essentially equal to the theoretical velocity (V_{th}) obtained by an isentropic expansion from the total inlet pressure (P_{Ti}) to the static discharge pressure (P_{sd}) at the discharge of the cascade. Assuming a constant discharge pressure (P_{sd}) and constant flow angles at the discharge, the mass flow rate ($\dot{m}$) for each unit of blade height can be determined with the equation (using the symbols of Figure B-1)

$$\dot{m} = \rho_{th} V_{th} \left[a - (\delta_1 + \delta_2) \right] + \sum \int_0^{\delta} u \rho \, dy .$$

Where the sum indicates that the integral has to be taken for both boundary layers, with the symbol η being equal to y/δ , the equation becomes

$$\dot{m} = \rho_{th} V_{th} \, a \left[1 - \sum \frac{\delta}{a} \left(1 - \int_0^1 \frac{u}{V_{th}} \frac{\rho}{\rho_{th}} \, d\eta \right) \right] . \qquad B(1)$$

With $\rho = p/RT$, and since the static pressure is assumed to be constant in the throat section, the following relationship occurs (using the symbols of the nomenclature in this Appendix):

$$\frac{\rho}{\rho_{th}} = \frac{T_{th}}{T} = \frac{1 - X_e}{1 - X_e (u/V_{th})^2} , \qquad B(2)$$

where $$X_e = 1 - \left(\frac{P_{sd}}{P_{Ti}} \right) \frac{\gamma - 1}{\gamma} \qquad B(3)$$

(1) Vavra, M. H., M-1 Fuel Turbine Aerodynamic Design, RMR No. C143, Aerojet-General Corporation, November 1963

For the turbulent boundary layers in turbomachines, the velocity distribution u/V_{th} will have the form

$$\frac{u}{V_{th}} = \left(\frac{y}{\delta}\right)^X = \eta^X , \qquad B(4)$$

where X is a constant.

Introducing equations B(2) and B(4) into equation B(1) results in

$$\mathring{m} = \rho_{th} V_{th} \; a \left\{1 - \sum \frac{\delta}{a}\left[1 - (1 - X_e)\int_o^1 \frac{\eta^X}{1 - X_e \eta^{2X}} d\eta\right]\right\}. \qquad B(5)$$

Let $\delta^* = \sum \delta\left[1 - (1 - X_e)\int_o^1 \frac{\eta^X}{1 - X_e \eta^{2X}} d\eta\right]$, and it follows B(6)

that equation B(5) can then be expressed by

$$\mathring{m} = \rho_{th} V_{th} \; a\varphi = \rho_{th} V_{th} \; a \left[1 - \sum \frac{\delta^*}{a}\right]. \qquad B(7)$$

φ is the restriction factor and is equal to $1 - \sum \frac{\delta^*}{a}$.

III. ENERGY LOSSES DUE TO BOUNDARY LAYERS

Using the symbols of Figure B-1 of this appendix, the total kinetic energy (KE) available at the cascade exit for each unit of blade height is

$$KE = \rho_{th} V_{th} \left[a - \sum \delta\right] \frac{V_{th}}{2gJ} + \sum \int_o^1 u\rho \frac{u^2}{2gJ} dy.$$

Using the equations B(2) and B(4), KE is equal to

$$\rho_{th} V_{th} \; a \; \frac{V_{th}}{2gJ} \left\{1 - \sum \frac{\delta}{a}\left[1 - (1 - X_e)\int_o^1 \frac{\eta^{3X}}{1 - X_e \eta^{2X}} d\eta\right]\right\}. \qquad B(9)$$

The so-called energy thickness (δ^{***}) of the boundary layers on both sides of a profile will be defined by

$$\delta^{***} = \sum \delta \left[1 - (1 - X_e) \int_0^1 \frac{\eta^{3X}}{1 - X_e \eta^{2X}} d\eta \right] . \qquad B(10)$$

Therefore, equation B(9) can be rewritten as

$$KE = \rho_{th} \frac{V_{th}^3}{2gJ} a \left(1 - \frac{\delta^{***}}{a}\right). \qquad B(11)$$

It is customary in turbine analyses to introduce the average discharge velocity (V_d) for the calculation of the efficiency of a cascade. The actual kinetic energy of the flow after the cascade is then

$KE = \mathring{m} \frac{V_d^2}{2gJ}$ where $\mathring{m}$ is the actual flow rate passing through a blade channel. By using equation B(7) to replace $\mathring{m}$, KE becomes

$KE = \rho_{th} V_{th} a \varphi \frac{V_d^2}{2gJ}$. Equating this expression with Equation B(11) and using equation B(8)

$$\left(\frac{V_d}{V_{th}}\right)^2 = \frac{1 - \sum \frac{\delta^{***}}{a}}{1 - \sum \frac{\delta^*}{a}} = 1 - \zeta , \qquad B(12)$$

where ζ is the usually applied energy loss coefficient for the calculations of a cascade.

IV. RELATIONSHIP BETWEEN FLOW RESTRICTION FACTOR AND LOSS COEFFICIENT[2]

$$\text{LET } H^{***} = \frac{\delta^{***}}{\delta^*} \qquad B(13)$$

For the definite value of γ and exponent X, the factor H^{***} can be determined as a function of the pressure ratio (P_{Ti}/P_{sd}) of the cascade. According to N. M. Markov[2] an exponent X of 0.15, represents a good average value for the turbulent boundary layers in turbine cascades at moderate Reynolds numbers.

---

(2) Markov, N. M., Calculation of the Aerodynamic Characteristics of Turbine Blading, Associated Technical Services Incorporated, Glen Ridge, New Jersey, 1958

Figure B-2 of this appendix shows the values of H*** for a γ of 1.37 and an X of 0.15 for the various pressure ratios. These data are obtained by expressing the integrands of equations B(6) and B(10) by binominal series, and then integrating them by parts.

The restriction factor φ of equation B(8) can now be expressed by the energy loss coefficient ζ as

$$\varphi = 1 - \sum \frac{\delta^*}{a} = \frac{H^{***} - 1}{H^{***} - 1 + \zeta} \quad . \qquad B(14)$$

For critical pressure ratios with a γ of 1.37, the value of H*** is 2.045. Therefore

$$\varphi_c = \frac{1.045}{1.045 + \zeta} = 1 - \frac{\zeta}{1.045 + \zeta} \qquad B(15)$$

The values of φ_c for different loss coefficients are

ζ =	0	0.05	0.10	0.15	0.20
φ_c =	1.0	0.954	0.912	0.874	0.839

V. FLOW AREA CALCULATIONS WITH POLYTROPIC PROCESS

It is often convenient to calculate the flow areas of a turbine by the equation

$$\phi^* = \frac{\dot{m}(T_T R)^{1/2}}{P_T A(g)^{1/2}} = \left\{ \frac{2\gamma}{\gamma - 1} \left[\left(\frac{P_S}{P_T}\right)^{2/n} - \left(\frac{P_S}{P_T}\right)^{n+1/n} \right] \right\}^{1/2} , \qquad B(16)$$

where the polytropic exponent $n = \frac{\gamma}{1 + \zeta_a (\gamma - 1)}$. B(17)

It must now be determined what loss coefficients should be introduced in equation B(17) to obtain flow rates through the particular areas that correspond with those obtained from equation B(7). Denoting the flow function of equation B(16) for friction-less expansion by ϕ_o^*, and that for a particular loss coefficient ζ_a by ϕ^*, the result must be

$$\phi^* = \varphi \, \phi_o^*$$

M. H. Vavra has established a computer program that calculates the flow functions (ϕ^*) of equation B(16) for various values of γ and pressure ratios. The program accounts for the effects of reheat. In other words, the polytropic loss coefficients that are introduced in equation B(17) are changed until the over-all loss coefficients with reheat correspond to the values for which ϕ^* is to be obtained. Using these tables for the critical pressure ratio with γ of 1.37, the following relation is obtained between the coefficients ζ for energy loss and the coefficients ζ_a for area calculations:

ζ =	0	0.05	0.10	0.15	0.20
ζ_a =	0	0.067	0.113	0.184	0.237

NOMENCLATURE FOR APPENDIX B

SYMBOL		UNITS
A	Area	$in.^2$
a	Throat Width	in.
Cp	Specific heat at constant pressure	$btu/lb_m\text{-}°R$
g	Acceleration due to gravity	ft/sec^2
H***	Energy factor of boundary layer	---
J	Mechanical equivalent of heat	ft-lb/btu
$\dot{m}$	Mass flow rate	lb_m/sec
n	Polytropic exponent = $\frac{\gamma}{1 + \zeta_a(\gamma - 1)}$	---
P_T	Total absolute pressure	psia
P_s	Static absolute pressure	psia
R	Gas constant	$ft/lb/lb_m\text{-}°R$
s	Spacing of blades	in.
T	Static temperature	°R
T_T	Total temperature	°R
u	Velocity in boundary layer	ft/sec
V	Absolute velocity	ft/sec
X	Constant	---
X_e	$1 - \left(\frac{P_{sd}}{P_{Ti}}\right)^{\frac{\gamma - 1}{\gamma}}$	---
y	Distance in boundary layer	in.
γ	Ratio of specific heats Cp/Cv	---
δ	Leakage Gap	in.

SYMBOL		UNITS
δ^*	Displacement thickness of boundary layer	in.
δ^{***}	Energy thickness of boundary layer	in.
ζ	Loss coefficient for efficiency	---
ζ_a	Loss coefficient for area calculations	---
η	Length ratio	---
η_T	Turbine efficiency	---
ρ	Mass density	lb_m/ft^3
ϕ^*	Flow function	---
φ	Restriction factor	---
φ_c	Restriction factor for critical pressure ratio	---

SUBSCRIPTS

0	Refers to inlet conditions
1	Refers to station after stator
2	Refers to station after rotor
i	Refers to inlet
d	Refers to discharge
is	refers to isentropic conditions
m	Refers to mean diameter
th	refers to theoretical conditions

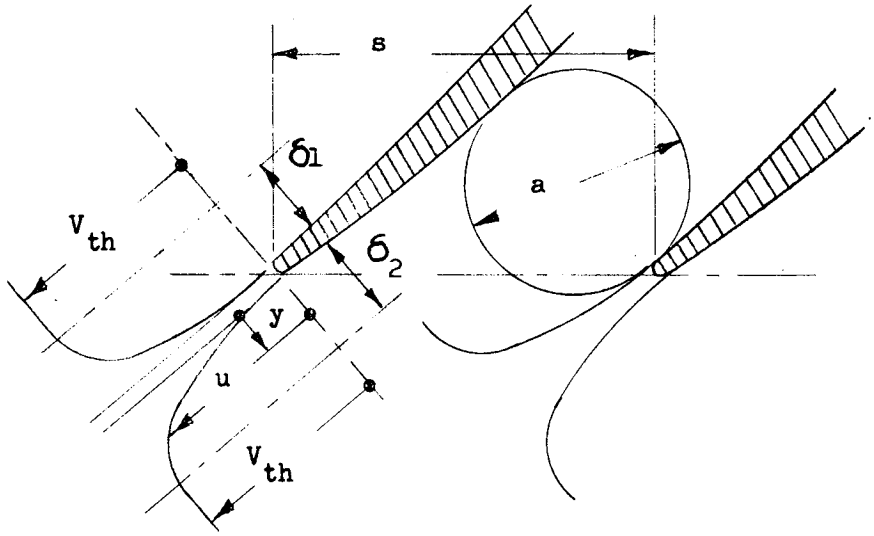

FIG. B-1A FLOW CONDITION AT CASCADE DISCHARGE

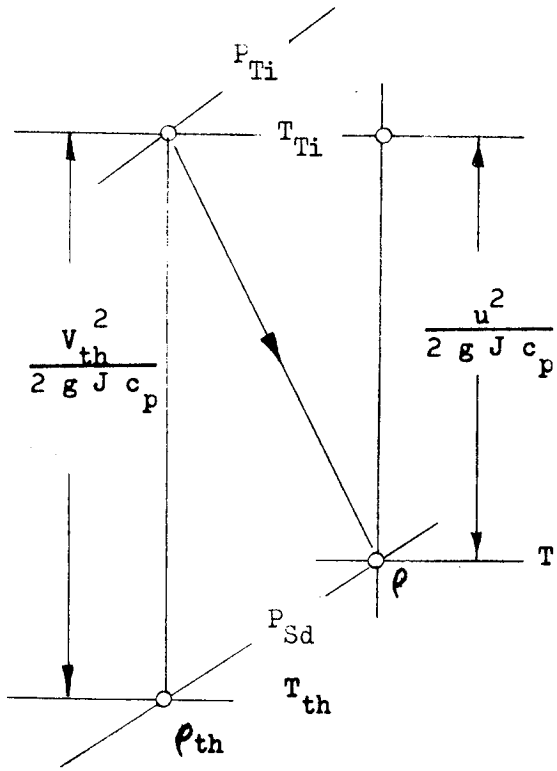

FIGURE B-1

ENTROPY DIAGRAM

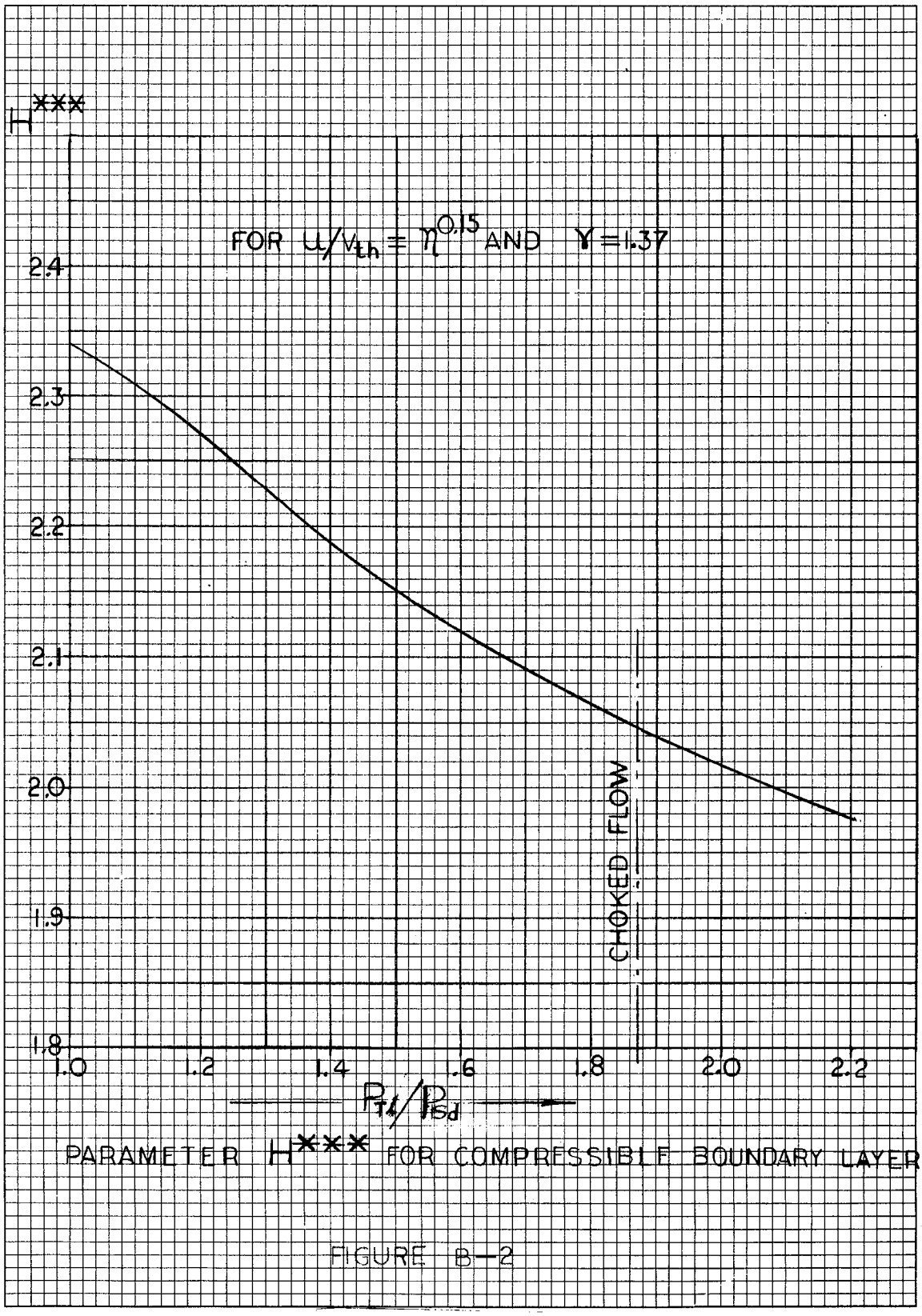

PARAMETER H^{***} FOR COMPRESSIBLE BOUNDARY LAYER

FIGURE B—2

APPENDIX C

TESTS OF THE CURVED SUPERSONIC NOZZLE

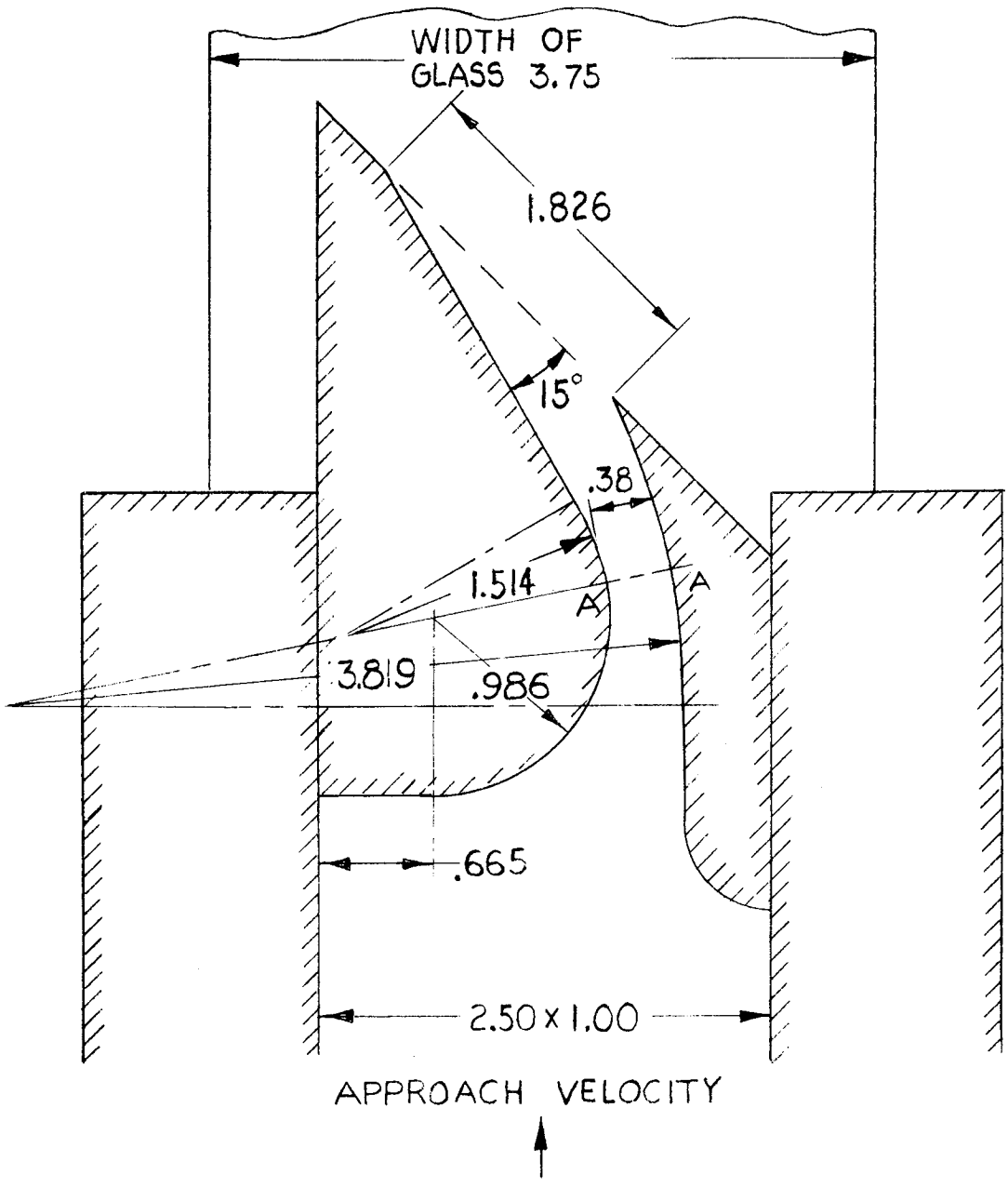

FIGURE C-1

SCHEMATIC OF TEST SET-UP

TESTS OF THE CURVED SUPERSONIC NOZZLE

During the preliminary design phase of the M-1 fuel turbine, tests could not be made with a full scale cascade of the nozzles for the first stage.

To prove the theoretical performance of the curved supersonic nozzle, Dr. Vavra[1] conducted tests with a full-size single nozzle in a small blow-down tunnel at the United States Naval Postgraduate School in Monterey, California.

Because of the small size of the tunnel, only the discharge portion of the nozzle could be tested. Figure C-1 of this appendix shows the configuration of the nozzle which was tested. It should be noted that the dimensions correspond to the actual nozzle profile of Figure 6 in Section III of this report. The approach section is 2.5-in. by 1.0-in., hence the flow is accelerated from an area of 2.5-in.^{2} at the inlet to 0.38-in.^{2} at the throat. The modified inlet section of the test nozzle should not influence the flow either ahead of or downstream of the throat.

Figures C-2 through C-5 of this appendix show Schlieren photographs at pressure ratios of 2.02, 3.04, 4.07 and 5.08, respectively. The flow pattern shown in Figure C-4 of the subject photographs is similar to the conditions that occur at the design point of the M-1 fuel turbine. It is apparent that the nozzle operates without separations and that it does not exhibit an excessive boundary layer growth. The 15.5 degree angle of the flow as it leaves the concave side of the nozzle is the same angle as that found through the theoretical considerations.

In Figure C-5 of this appendix it should be noted that after-expansions are associated with flow deflections. This is evident from the measured flow angle and the large fans of expansion and compression waves. At a pressure ratio of 2.02, as shown in Figure C-2 of this appendix, the normal shock pattern occurs at the nozzle exit. When the pressure ratio is increased to 3.04, as shown in Figure C-3 of this appendix, the shock pattern moves downstream of the exit.

These tests have shown that the curved divergent-convergent nozzles perform according to theoretical predictions, and that, for the pressure ratio required, they are superior to a convergent nozzle with large after-expansions.

---

(1) Vavra, M. H., M-1 Fuel Turbine, Aerodynamic Design, RMR No. 0143, Aerojet-General Corporation, November 1963

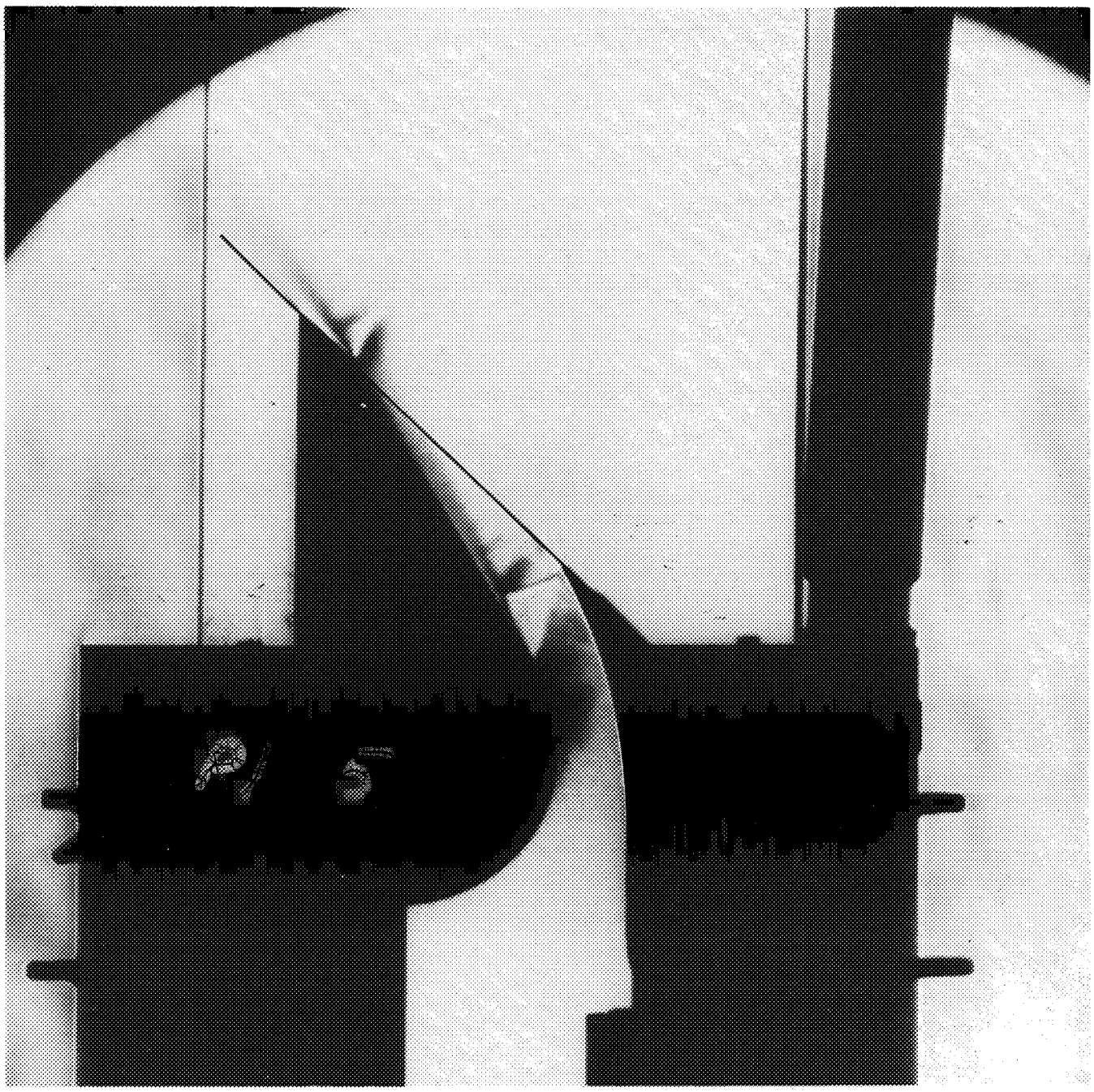

SCHLIEREN PHOTOGRAPH OF NOZZLE TEST
AT PROPULSION LABORATORY, USNPGS,
MONTEREY, CALIFORNIA

INLET PRESSURE = 15 psig
PRESSURE RATIO = 2.02

FIGURE C-2

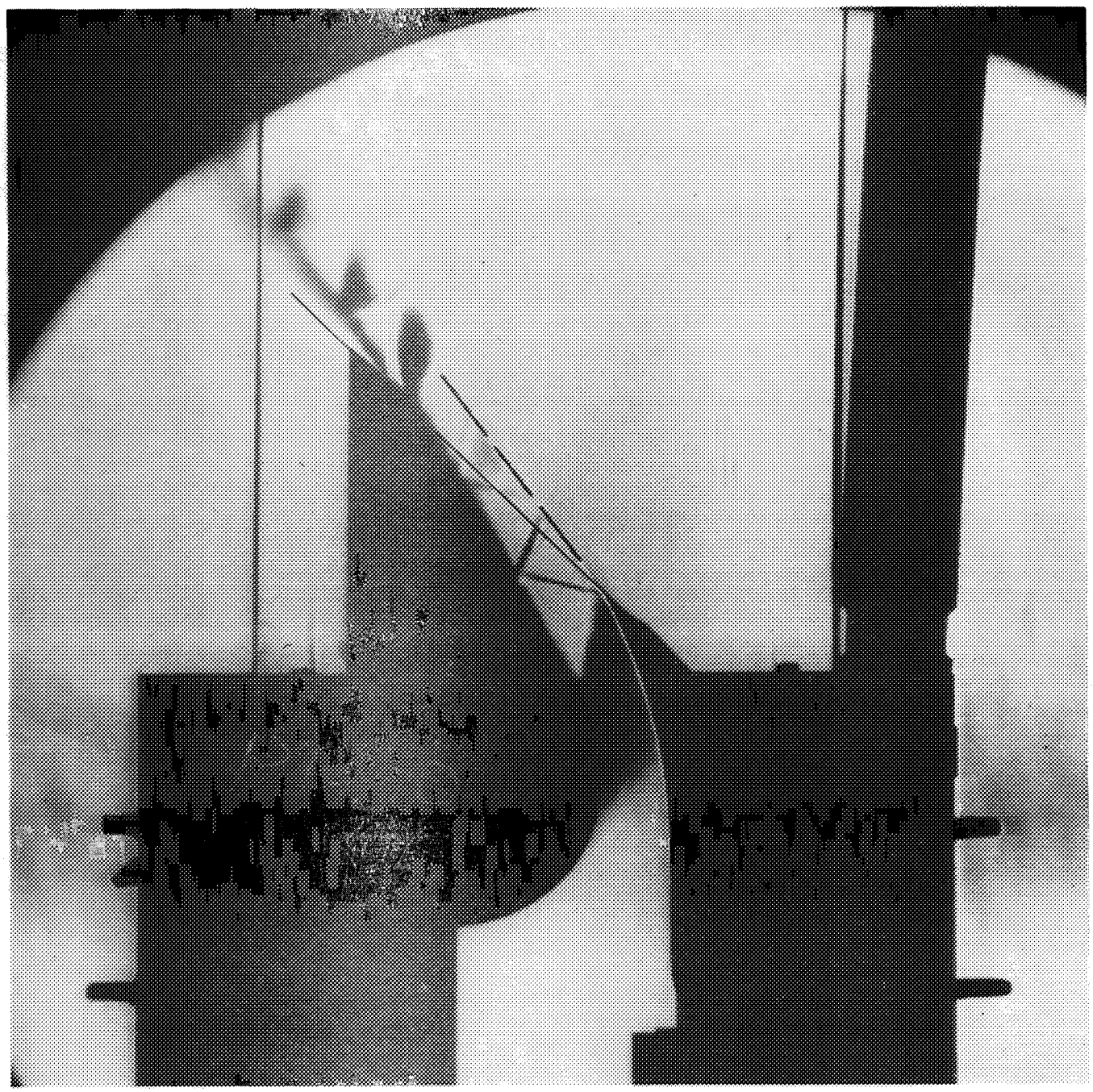

SCHLIEREN PHOTOGRAPH OF NOZZLE TESTS
AT PROPULSION LABORATORY, USNPGS,
MONTEREY, CALIFORNIA

INLET PRESSURE = 30 psig
PRESSURE RATIO = 3.04

FIGURE C-3

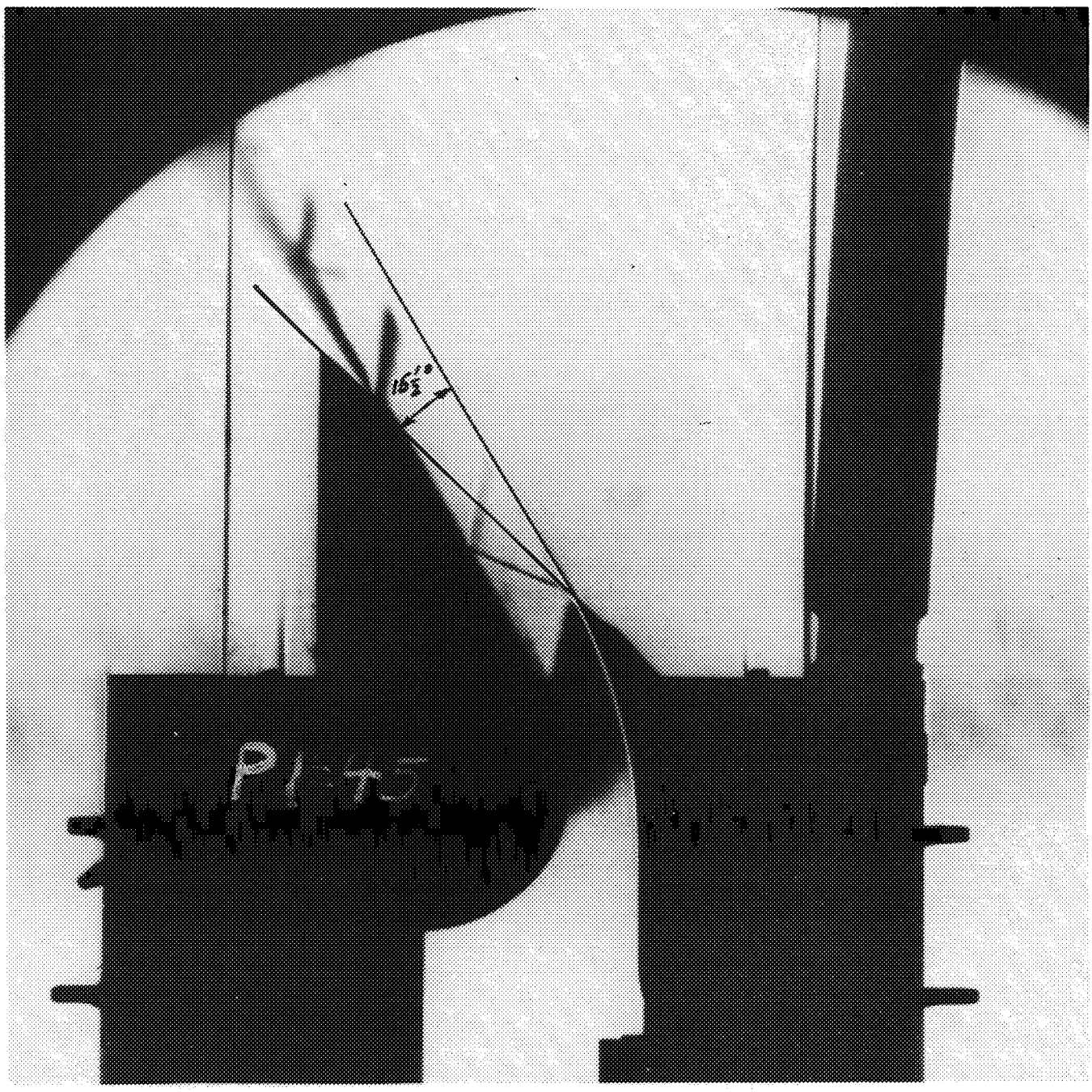

SCHLIEREN PHOTOGRAPH OF NOZZLE TEST
AT PROPULSION LABORATORY, USNPGS,
MONTEREY, CALIFORNIA

INLET PRESSURE = 45 psig
PRESSURE RATIO = 4.07

FIGURE C-4

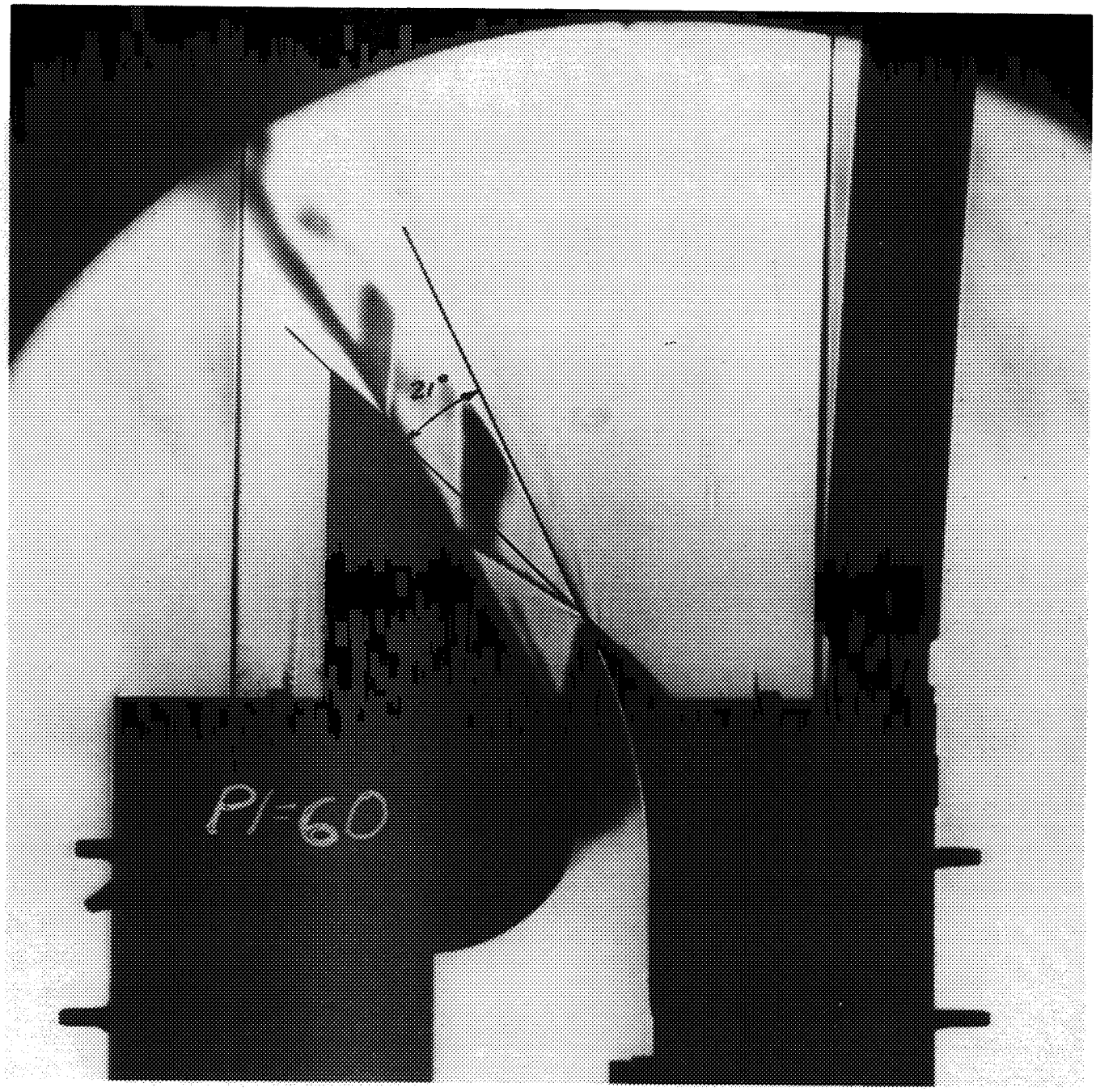

SCHLIEREN PHOTOGRAPH OF NOZZLE TEST
AT PROPULSION LABORATORY, USNPGS,
MONTEREY, CALIFORNIA

INLET PRESSURE = 60 psig
PRESSURE RATIO = 5.08

FIGURE C-5

REPORT NASA CR 54820 DISTRIBUTION LIST

W. F. Dankhoff (5 Copies)
NASA
Lewis Research Center
21000 Brookpark Road
Cleveland, Ohio 44135
Mail Stop 500-305

J. A. Durica (1 Copy)
Mail Stop 500-210

Patent Counsel (1 Copy)
Mail Stop 77-1

Lewis Library (2 Copies)
Mail Stop 62-1

Lewis Technical Information
Division (1 Copy)
Mail Stop 5-5

M. J. Hartmann (1 Copy)
Mail Stop 5-9

W. L. Stewart (1 Copy)
Mail Stop 5-9

J. C. Montgomery (1 Copy)
Mail Stop 501-1 SNPO-C

Major E. H. Karalis (1 Copy)
AFSC Liaison Office
Mail Stop 4-1

Lewis Office of Reliability and
Quality Assurance (1 Copy)
Mail Stop 500-203

NASA Representative (6 Copies)
NASA Scientific and Technical
Information Facility
Box 5700
Bethesda, Maryland

Library (1 Copy)
NASA
Ames Research Center
Moffett Field, California 94035

Library (1 Copy)
NASA
Flight Research Center
P. O. Box 273
Edwards AFB, California 93523

Library (1 Copy)
NASA
Goddard Space Flight Center
Greenbelt, Maryland 20771

Library (1 Copy)
NASA
Langley Research Center
Langley Station
Hampton, Virginia 23365

Library (1 Copy)
NASA
Manned Spacecraft Center
Houston, Texas 77058

Library (1 Copy)
NASA
George C. Marshall Space Flight Center
Huntsville, Alabama 35812

Library (1 Copy)
NASA
Western Operations
150 Pico Boulevard
Santa Monica, California 90406

Library (1 Copy)
Jet Propulsion Laboratory
4800 Oak Grove Drive
Pasadena, California 91103

A. O. Tischler (2 Copies)
NASA Headquarters
Code RP
Washington, D. C.

J. W. Thomas, Jr. (5 Copies)
NASA
George C. Marshall Space Flight Center
I-E-E
Huntsville, Alabama

E. W. Gomersall (1 Copy)
NASA
Mission Analysis Division
Office of Advanced Research and Technology
Moffett Field, California 94035

Dr. Keith Boyer (1 Copy)
Los Alamos Scientific Laboratory
CMF-9
P. O. Box 1663
Los Alamos, New Mexico

Dr. G. Wislicenus (1 Copy)
Penn. State University
Naval Ordinance Laboratory
University Park, Pennsylvania

Dr. A. Acosta (1 Copy)
California Institute of Technology
1201 East California Street
Pasadena, California

Dr. E. B. Konecci (1 Copy)
National Aeronautics and Space Council
Executive Office of the President
Executive Office Building
Washington, D. C.

Dr. M. Vavra (1 Copy)
Naval Post Graduate School
Monterey, California

H. V. Main (1 Copy)
Air Force Rocket Propulsion Laboratory
Edwards Air Force Base
Edwards, California

Dr. George Serovy (1 Copy)
Iowa State University
Ames, Iowa

T. Iura (1 Copy)
Aerospace Corporation
2400 East El Segundo Boulevard
P. O. Box 95085
Los Angeles, California 90045

F. Ghahremani (1 Copy)
Aerospace Corporation
2400 East El Segundo Boulevard
P. O. Box 95085
Los Angeles, California 90045

Chemical Propulsion Information Agency
(1 Copy)
Johns Hopkins University
Applied Physics Laboratory
8621 Georgia Avenue
Silver Springs, Maryland

Robert O. Bullock (1 Copy)
Garrett Corporation
Airesearch Manufacturing Division
402 S. 36th Street
Phoenix, Arizona 85034

REPORT NASA CR 54820 DISTRIBUTION LIST

(Continued)

Pratt and Whitney Aircraft Corporation
(1 Copy)
Florida Research and Development Center
P. O. Box 2691
West Palm Beach, Florida 33402

Rocketdyne (Library Department 586-306)
(1 Copy)
Division of North American Aviation
6633 Canoga Avenue
Canoga Park, California 91304

John Stanitz (1 Copy)
Thompson Ramo Wooldridge, Inc.
23555 Euclid Avenue
Cleveland, Ohio 44117

Dr. M. J. Zucrow (1 Copy)
Purdue University
Lafayette, Indiana 47907